Taxon-specific phytoplankton growth, nutrient utilization, and

light limitation in the oligotrophic Gulf of Mexico NATALIA YINGLING1*, THOMAS B. KELLY1, TAYLOR A. SHROPSHIRE1, MICHAEL R. LANDRY², KAREN E. SELPH³, ANGELA N. KNAPP¹, SVEN A. KRANZ¹, MICHAEL R. STUKEL¹ ¹ DEPARTMENT OF EARTH, OCEAN AND ATMOSPHERIC SCIENCE, FLORIDA STATE UNIVERSITY, TALLAHASSEE, FL 32306, USA ² SCRIPPS INSTITUTION OF OCEANOGRAPHY, 9500 GILMAN DR., LA JOLLA, CA 92093-0227, USA ³ DEPARTMENT OF OCEANOGRAPHY, UNIVERSITY OF HAWAII AT MANOA, HONOLULU, HI 96822, USA * CORRESPONDING AUTHOR: Natalia Yingling (ny18b@my.fsu.edu) **Keywords:** new production, recycled production, half-saturation, photosynthesis-irradiance, nutrient kinetics

ABSTRACT

The highly stratified, oligotrophic regions of the oceans are predominantly nitrogen limited in the surface ocean and light limited at the deep chlorophyll maximum (DCM). Hence, determining light and nitrogen co-limitation patterns for diverse phytoplankton taxa is crucial to understanding marine primary production throughout the euphotic zone. During two cruises in the deep-water Gulf of Mexico, we measured primary productivity (H¹³CO₃-), nitrate uptake (¹⁵NO₃⁻), and ammonium uptake (¹⁵NH₄⁺) throughout the water column. Primary productivity declined with depth from the mixed-layer to the DCM, averaging 27.1 mmol C m⁻² d⁻¹. The fraction of growth supported by NO₃ was consistently low, with upper euphotic zone values ranging from 0.01 to 0.14 and lower euphotic zone values ranging from 0.03 to 0.44. Nitrate uptake showed strong diel patterns (maximum during the day), while ammonium uptake exhibited no diel variability. To parameterize taxon-specific phytoplankton nutrient and light utilization, we used a data assimilation approach (Bayesian Markov Chain Monte Carlo) including primary productivity, nutrient uptake, and taxon-specific growth rate measurements. Parameters derived from this analysis define distinct niches for five phytoplankton taxa (Prochlorococcus, Synechococcus, diatoms, dinoflagellates, and prymnesiophytes) and may be useful for constraining biogeochemical models of oligotrophic open-ocean systems.

INTRODUCTION

53

54

55

56

57

58

59

60

61

62

63

64

65

66

67

68

69

70

71

72

73

74

75

76

77

78

79

80

81

82

Nutrient acquisition by phytoplankton is an important factor regulating marine primary productivity (Davey et al., 2008; Duce et al., 2008; Mulholland and Lomas, 2008). The openocean Gulf of Mexico (GoM) is a highly-stratified, oligotrophic region where the Loop Current, mesoscale eddies and episodic storm events influence lateral and vertical transport of nutrients and organisms (Biggs, 1992; Forristall et al., 1992; Biggs and Ressler, 2001; Oey et al., 2005). These features create dynamic ecological mosaics with substantial mesoscale spatial variability in the phytoplankton community (Biggs and Müller-Karger, 1994; Gomez et al., 2018). Intense stratification also leads to deep chlorophyll maxima (DCM) that potentially provide unique niches for phytoplankton compared to low-nutrient, high-light environments found in the shallow mixed-layer (Shropshire et al., 2020; Knapp et al., this issue; Selph et al., this issue). Additionally, the oligotrophic GoM is an important spawning region for economically-valuable and environmentally-important nekton, including Atlantic Bluefin Tuna (Rooker et al., 2007; Cornic et al., 2008). In addition to vertical advection, previous studies have found that nitrogen fixation, NO₃ upwelling along the boundaries of mesoscale eddies, and horizontal advection of nutrients can be important nitrogen sources in the GoM (Walker et al., 2005; Mulholland et al., 2006). While the sources of bioavailable nitrogen in the oligotrophic GoM are likely spatiotemporally variable, a more accurate understanding of phytoplankton nutrient-uptake dynamics is important to provide insight into what regulates group-specific community composition and inform future biogeochemical models. Variability in phytoplankton ecophysiology adds complexity to the basic processes of

Variability in phytoplankton ecophysiology adds complexity to the basic processes of primary productivity in pelagic habitats. *Prochlorococcus* is often the dominant phytoplankton taxon in oligotrophic regions (Chisholm *et al.*, 1988; Partensky *et al.*, 1999); however, many ecotypes of this genus exist, with different nutrient uptake capabilities and consequently biogeochemical impacts (Zwirglmaier et al., 2008; Martiny *et al.*, 2009; Kashtan *et al.*, 2014; Kent *et al.*, 2016; De Martini *et al.*, 2018). *Prochlorococcus* is the numerically dominant phytoplankton in our study region and comprises roughly half of the total carbon-based biomass (Selph *et al.*, this issue). *Synechococcus* and picoeukaryotes (especially prymnesiophytes, chlorophytes, and pelagophytes) are also important, with picoeukaryotes comprising a larger portion of biomass with increasing depth (Selph *et al.*, this issue). Since different phytoplankton

groups, as well as species and ecotypes within groups, differ in their adaptations for life in nutrient-depleted environments, their responses to dynamic environments may also be quantitatively and qualitatively different (Dutkiewicz *et al.*, 2013).

Constraining phytoplankton functional relationships (i.e., phytoplankton responses to environmental variables) is necessary to enable forecasting of ecological impacts in dynamic environments and modified physical conditions—such as those expected in a future ocean. Numerical modeling of marine microbial ecosystems is presently limited by an inability to accurately constrain *in situ* ecophysiological relationships amongst diverse phytoplankton taxa (Anderson, 2005; Franks, 2009; Follows and Dutkiewicz, 2011). Here, we address three questions aiming to better constrain group-specific functional phytoplankton relationships: 1) How do net primary production (NPP) and NO₃⁻ uptake rates of phytoplankton in the open-ocean GoM vary with depth and time of day; 2) What nitrogen sources support these phytoplankton; and 3) How do nutrient limitation and light limitation vary among different phytoplankton taxa?

Answers to these questions are derived from measurements collected during two field studies as part of the Bluefin Larvae in Oligotrophic Ocean Foodwebs: Investigating Nutrients to Zooplankton in the Gulf of Mexico (BLOOFINZ-GoM) project (Gerard *et al.*, this issue). Specifically, we conducted Lagrangian experiments with repeated depth-resolved measurements of NPP, nutrient uptake and taxon-specific phytoplankton growth rates, while also assessing the biomass of different phytoplankton. We then assimilate this field data to parameterize group-specific phytoplankton nutrient kinetics for application to biogeochemical models.

METHODS

Cruise structure and sampling strategy

Data are from two cruises in the open-ocean northern GoM (NF1704 in May, 2017; NF1802 in May, 2018) as part of the BLOOFINZ-GoM project. We conducted five Lagrangian experiments ('Cycles' referred to as C1, C2, C3, C4 and C5 to represent each cycle) lasting 2-4 days each (Gerard *et al.*, this issue). Each cycle used a pair of satellite-tracked marker buoys tethered to subsurface drogues to follow the mixed-layer in a Lagrangian frame of reference (Landry *et al.*, 2009; Stukel *et al.*, 2015). One array ("incubation array") included attachment points for mesh bags containing incubation bottles for NO₃- uptake, NPP, and taxon-specific

phytoplankton growth and grazing rates at depths spanning the euphotic zone. The Lagrangian approach permitted repeated sampling of the same water parcel to quantify variability in phytoplankton biomass and rates over the duration of each cycle. Samples for fluorometric chlorophyll *a* (Strickland and Parsons, 1972), phytoplankton biomass (Selph *et al.*, this issue), nutrients (NO₃⁻ and NH₄⁺, Knapp *et al.*, this issue), and *in situ* incubation experiments were collected at 6 depths from the surface to the DCM on daily 02:00 a.m. (local U.S. central) CTD-Niskin rosette casts. Samples for shipboard incubations were collected from daily CTD casts near dusk. For more detail on sampling methodology see the aforementioned studies in this issue.

Phytoplankton community composition and biomass

112

113

114

115

116

117

118

119

120

121

122

123

124

125

126

127

128

129

130

131

132

133

134

135

136

137

138

139

140

141

As reported in Selph et al. (this issue), we quantified phytoplankton abundance using a combination of flow cytometry (FCM), epifluorescence microscopy (EPI), and high-pressure liquid chromatography (HPLC). Cells identified by FCM were categorized into three populations (*Prochlorococcus* (PRO), *Synechococcus* (SYN), and picoeukaryotes (PEUK)) based on forward-angle and side-angle light scattering and fluorescence signatures for DNA, phycoerythrin, and chlorophyll. For larger cells (i.e., diatoms (DIAT), autotrophic dinoflagellates (ADINO), prymnesiophytes (PRYM)), and other eukaryotes (OTHER), a combination of HPLC and EPI was used to determine taxa-specific biomass. HPLC-derived pigments were partitioned into taxonomic groups using CHEMTAX (Wright et al., 2008; Higgins et al., 2011; Selph et al., this issue). EPI samples from the shallowest two depths (within the mixed-layer, which we define as the depth at which density increases by 0.125 kg/m⁻³ (Monterey and Levitus, 1997)) and the deepest two depths (just above and at the DCM) from three of the Lagrangian cycles (C1, C4, and C5) were used to determine depth-varying carbon:chlorophyll ratios, hence, carbon-based biomass for each group. Assuming Redfield C:N ratios (106:16, mol:mol), carbon-based biomasses from Selph et al., (this issue) were converted to nitrogen-based biomasses for the biogeochemical model (Redfield 1963). See Supplemental Appendix A and Selph *et al.* (this issue) for additional details.

Phytoplankton growth, productivity, and grazing rates

We used three distinct incubation strategies for quantifying phytoplankton productivity and nutrient uptake rates: 24-h *in situ* incubations on the "incubation" array (NPP, NO₃ uptake,

and taxon-specific phytoplankton growth rates); 6-h shipboard incubations starting at dawn (vertical patterns of NO₃⁻ and NH₄⁺ uptake); and diel shipboard incubations consisting of sequential 4-h incubations for 24 h (diurnal patterns of NO₃⁻ and NH₄⁺ uptake).

Taxon-specific growth rates - Two-point seawater dilution grazing experiments were conducted *in situ* daily at 6 depths spanning the euphotic zone to determine taxon-specific phytoplankton growth rates for a total of 88 independent experiments (Landry *et al.*, 2008, 2011, this issue). 2.7-L samples of either whole seawater or partially diluted seawater (32% whole seawater/68% 0.1-μm filtered seawater) were incubated for 24-h on the incubation array. Initial and final samples for FCM (*Prochlorococcus* and *Synechococcus*), HPLC (dinoflagellates, diatoms and prymnesiophytes), and fluorometric chlorophyll *a* (bulk phytoplankton) were used to determine taxon-specific phytoplankton growth and mortality at each depth. See Supplementary Appendix A and Landry *et al.* (this issue) for additional details.

In situ NPP and nitrate uptake - NPP and ¹⁵NO₃⁻ uptake rates were measured at the same 6 depths on the incubation array. Four incubation bottles (2.7-L) per depth were filled from Niskin rosettes (three light bottles, one dark bottle). All bottles were spiked with H¹³CO₃⁻ (final concentration of 154 or 196 μmol L⁻¹ on NF1704 and NF1802, respectively). Two light bottles were spiked with ¹⁵NO₃⁻ (final concentration of 10 or 8 nmol L⁻¹ on NF1704 and NF1802, respectively). Bottles were then incubated for 24 h on the array. Upon recovery, incubations were immediately vacuum filtered onto pre-combusted 25-mm GF/F filters in the dark. Filters were rinsed with filtered seawater, wrapped in foil and stored at -80°C. Samples were fumigated with HCl vapor to remove inorganic carbon, dried, and placed inside a tin cup to be used for C/N and isotopic analysis at the University of California, Davis stable isotope facility. Uptake rates (¹⁵NO₃⁻ or bicarbonate) were determined for each incubation bottle using equations in Stukel (2020). NO₃⁻ uptake is reported as the average and uncertainty of the ¹⁵NO₃⁻ spiked bottles. As no statistically significant difference in H¹³CO₃⁻ uptake was detected between bottles spiked with ¹⁵NO₃⁻ and those without, NPP is reported as the average and uncertainty of H¹³CO₃⁻ uptake in the three light bottles corrected for dark bottle H¹³CO₃⁻ uptake.

Shipboard vertically-resolved nitrate and ammonium uptake - Since NH₄⁺ recycling within 24-h bottle incubations can substantially bias measurements of NH₄⁺ uptake (Dugdale and Wilkerson, 1986), we conducted short-term (6-h) NH₄⁺ and NO₃⁻ uptake experiments in

shipboard incubators. Each incubator was uniformly shaded using clear or blue-tinted acrylic sheets to achieve three light levels as determined by simultaneous measurements with a $2-\pi$ LICOR photosynthetically active radiation (PAR) sensor for downwelling irradiance and a $4-\pi$ water-proof LI-COR PAR sensor for ambient irradiance in the incubator. These calibrations were done shipboard to account for light reflection or shading effects specific to their location. Incubation light levels for NF1704 (C1-C3) were determined to be 145% (clear, surface), 79% (mixed-layer), and 21% (lower mixed-layer) of surface irradiance (I₀). For NF1802 (C4-C5), the clear incubator was replaced with one screened to 1.7% I₀ to mimic DCM light. Incubators were cooled with mixed-layer seawater (24.5-26.5°C). Samples were drawn from depths near these light levels (as determined from noon CTD casts with CTD-mounted PAR sensor).

To determine patterns of nitrate and ammonium uptake as a function of depth, six 2.7-L samples from each of the three incubator light levels (e.g., 5, 15, and 45 m for surface, 79% and 21% I₀, respectively) were collected near dusk and placed in the incubators until dawn (N.B., ship schedule and CTD water budget did not allow dawn sampling for these experiments). At dawn, triplicate samples from each depth were spiked with either ¹⁵NO₃- or ¹⁵NH₄+ (concentrations as above) and incubated for 6-h (dawn to approximately local noon). Samples were then filtered and analyzed as described above.

Shipboard diel nitrate and ammonium uptake experiments - To determine diel variability in nutrient uptake and assess potential recycling occurring within 24-h incubations, we also conducted short-term (diurnally-resolved) nutrient uptake experiments. Nine to twelve 2.7-L bottles were filled at dusk. Two or three 24-h reference bottles (24-h incubation) and an additional "time point" bottle (4-h incubation) were immediately spiked with ¹⁵NO₃- or ¹⁵NH₄+ (the remainder of the bottles were not immediately spiked). All bottles were then returned to the incubator. After ~4 h, the first experimental bottle was removed from the incubator and filtered, and a second experimental bottle was spiked. This process continued for 24-h to produce six sequential 4-h incubations from which diurnal patterns of nutrient uptake could be determined. After 24-h, the reference bottles were harvested. No diel experiments were conducted during C3 (NF1704), and no diel ammonium uptake experiments were conducted during C4 (NF1802). On all other cycles (C1, C2, C5), simultaneous NO₃- or NH₄+ uptake diel experiments were conducted. On NF1802 (C4-C5), diel experiment bottles were also spiked with H¹³CO₃- to simultaneously determine diel variability in NPP.

Data assimilation and model parameterization

- Model Structure—Phytoplankton growth is parameterized using transfer functions from the biogeochemical model NEMURO-GoM (Shropshire *et al.*, 2020; Shropshire *et al.*, this issue), which was designed for the open-ocean GoM. NEMURO-GoM parameterizes phytoplankton growth as a function of light, nutrients and temperature. By default, it includes two phytoplankton groups (small (SP) and large (LP)); however, we extended this model to parameterize 6 distinct groups that were identifiable through FCM, HPLC and/or EPI approaches above: (1) PRO, (2) SYN, (3) PRYM, (4) ADINO, (5) DIAT and (6) OTHER (equaling the residual biomass from the remaining groups of autotrophic eukaryotic phytoplankton).
 - NEMURO-GoM parameterizes group-specific growth rates with the following 7 equations: (1) NO₃⁻ limitation (NL), (2) NH₄⁺ limitation (AL), (3) light limitation (LL), (4) temperature limitation (TL), (5) respiration (Resp), (6) gross primary productivity (GPP), and (7) NPP, wherein K_{NO3} is the NO₃⁻ half-saturation constant (μM), K_{NH4} is the NH₄⁺ half-saturation constant (μM), α is the initial slope of the photosynthesis-vs-irradiance curve (m² W⁻¹ d⁻¹), β is the light-inhibition constant (m² W⁻¹ d⁻¹), and V is the maximum-specific-growth rate at a reference temperature (d⁻¹). NEMURO-GoM uses a reference temperature of 0°C, but we provide values referenced to 25°C, which is representative of the GoM mixed-layer during our cruises. Q is the temperature effect coefficient (°C⁻¹), R is biomass-specific respiration, E is growth-specific excretion, and B is biomass (mmol N m⁻³). Subscript "*i*" indicates group-specific parameters with nitrate concentrations (μM, [NO₃⁻]), ammonium concentrations (μM, [NH₄⁺]), PAR, and T (°C) as environmental conditions. For our Bayesian parameter-selection procedure (see below), all group-specific parameters except β were log transformed. Equations are as follows:

226
$$NL_i = \frac{[NO_3^-]}{[NO_2^-] + K_{NO2}i} \cdot \left(1 + \frac{[NH_4^+]}{K_{NH4}i}\right)^{-1}$$
 (Eq. 1)

227
$$AL_i = \frac{[NH_4^+]}{[NH_4^+] + K_{NH4,i}}$$
 (Eq. 2)

228
$$LL_i = \left(1 - \exp\left(\frac{-\alpha_i \cdot PAR}{V_i}\right)\right) \cdot \exp\left(\frac{-\beta_i \cdot PAR}{V_i}\right)$$
 (Eq. 3)

$$229 TL_i = \exp(Q \cdot T) (Eq. 4)$$

$$230 Resp_i = R_i \cdot \exp(Q \cdot T) (Eq. 5)$$

231
$$GPP_i = V_i \cdot B_i \cdot (NL_i + AL_i) \cdot LL_i \cdot TL_i$$
 (Eq. 6)

$$NPP_i = GPP_i \cdot (1 - E_i) - Resp_i \cdot B_i$$
 (Eq. 7)

- 233 Bayesian Parameter Optimization Procedure—To constrain group-specific model parameters,
- 234 we used a Bayesian parameter-selection method applied to a modified 0-dimensional version of
- NEMURO-GoM consisting of Eq. 1-7 with 6 phytoplankton taxa (additional details in
- 236 Supplemental Appendix B). Our objective was not to find a single "best" parameterization, but
- rather to develop a statistical ensemble of possible parameter sets that reflects both uncertainty
- within the data and uncertainty in taxon-specific responses to light, temperature and nutrients.
- Briefly, the initial parameter set, τ_0 , is set to be equivalent to NEMURO-GoM default
- parameterizations for either SP or LP (Supplemental Table AI). The model is then initialized
- and run with *in situ* phytoplankton abundances, nutrient concentrations, temperature, and light
- 242 equivalent to the observed initial conditions for every *in situ* incubation experiment. A joint
- probability is then used to assess both the model-data misfit (sum-of-squared normalized
- residuals) between observations (NPP, NO₃ uptake, and taxon-specific growth rates) and model
- results (Eq. 8; "likelihood") and the prior probability of the parameter set used (Eq. 9).

246 Likelihood:
$$P(data|\tau) = \prod_{i \in data} \left(\frac{1}{\sigma_i \sqrt{2\pi}} \cdot e^{-\frac{1}{2} \left(\frac{x_i - x_t'}{\sigma_i} \right)^2} \right)$$
 (Eq. 8)

- where x_i and σ_i are the measurement and measurement uncertainty, respectively, of the *i*'th
- observation and x_{τ}' is the modeled value for that observation.

249 Prior probability:
$$P(\tau) = \prod_{t \in \tau} \left(\frac{1}{\sigma_t \sqrt{2\pi}} \cdot e^{-\frac{1}{2} \left(\frac{t - t^*}{\sigma_t} \right)^2} \right)$$
 (Eq. 9)

- where t^* and σ_t are the mean and standard deviation, respectively, for the prior estimate of model
- parameter value *t* (Supplemental Table AI).
- To explore the possible solution space, we used a Markov Chain Monte Carlo procedure
- with the Metropolis-Hastings algorithm (Hastings, 1970). For each iteration of the random walk,
- each parameter is varied by a small increment (in log-transformed space if a variable was

transformed) yielding a new parameter set: τ_{j+1} , which is used to re-run the model yielding a new likelihood and prior probability. The new parameter set would be "accepted" any time cost (i.e., $-P(data|\tau_{j+1}) \cdot P(\tau_{j+1})$) decreased and may be accepted even when cost increases based on the acceptance ratio: $\frac{-P(data|\tau_{j+1}) \cdot P(\tau_{j+1})}{-P(data|\tau_{j}) \cdot P(\tau_{j})}$. If the new parameter set is accepted, the random walk continues from τ_{j+1} . Otherwise a new τ_{j+1} is calculated. The first 50% of accepted parameter sets were removed ("burn-in") and the remainder were subsampled (1 in 50) to remove autocorrelation between parameter sets and yielding ~20,000 final parameter sets.

RESULTS

In situ conditions and the phytoplankton community

All five cycles had surface chlorophyll concentrations <0.2 μ g L⁻¹ and a pronounced DCM between 69 and 137 m (Girard *et al.*, this issue). The top of the DCM typically corresponded to ~1–2% I₀. NO₃⁻ concentrations were consistently <0.1 μ M at depths shallower than 69 m and generally <1 μ M throughout the entire euphotic zone (Knapp *et al.*, this issue). Only C5, with the shallowest euphotic zone and closest to the shelf break, had >1 μ M NO₃⁻ at <100 m depth.

Prochlorococcus averaged ~50% of the carbon-based phytoplankton biomass in all water parcels, although its proportional contribution varied from 31-66% of integrated euphotic zone biomass, being slightly more dominant in cycles with deeper DCMs (Table 2). PRO biomass typically increased with depth from the mixed-layer to a subsurface maximum slightly above the DCM before declining at the DCM. Mixed-layer SYN:PRO biomass ratios ranged from 0.2-1.4. However, SYN biomass decreased with depth, such that it represented ≤10% of PRO biomass at the DCM. Combined, cyanobacteria contributed a mean (\pm standard deviation) of 67 \pm 14% of euphotic zone integrated autotrophic carbon, while 2-10 μm eukaryotic cells comprised most of the remaining biomass. Prymnesiophytes were the dominant eukaryotic taxa, comprising 17 \pm 7%, while chlorophytes and pelagophytes represented 5 \pm 3% and 4.2 \pm 2%, respectively, of integrated euphotic zone carbon biomass. Diatoms were only minor contributors to autotrophic biomass (<2% in all cycles). For additional details on community composition, see Selph *et al.* (this issue).

Vertical profiles of NPP and nutrient uptake

NPP declined almost monotonically with depth on all cycles, although mixed-layer NPP was typically only 2 to 3-fold higher than NPP at the DCM (Fig. 1). NPP showed relatively weak inter-cycle variability. Cycle-average NPP varied from 0.27-0.55 μmol C L⁻¹ d⁻¹ at 5 m and varied from 0.10-0.29 μmol C L⁻¹ d⁻¹ at the DCM. The highest vertically integrated NPP (mean: 29.3 mmol C m⁻² d⁻¹) was for C5 (the cycle closest to the shelf), which also had the shallowest DCM, euphotic zone depth, and nitracline. The lowest vertically-integrated NPP was measured during C2 (24.3 mmol C m⁻² d⁻¹).

Vertical structure was less distinct for NO₃⁻ uptake rates (Fig. 1). Across depths and cycles, NO₃⁻ uptake typically ranged from 5-20 nmol N L⁻¹ d⁻¹. C1 exhibited a modest subsurface peak at 20-30 m (the rate was much higher for one outlier experiment at the DCM, likely due to contamination). C2 and C3 showed evidence for a weak subsurface maximum at ~60 m, while rates were relatively constant with depth for C4. C5 was the only cycle with a clear surface maximum in NO₃⁻ uptake rates. Vertically integrated, cycle-average NO₃⁻ uptake ranged from 0.72 (C4) to 3.45 mmol N m⁻² d⁻¹ (C1).

To investigate the relative proportion of NPP supported by NO₃⁻ uptake (commonly referred to as the *f*-ratio), we computed an *f*-ratio from *in situ* data as:

$$f_{is} = \frac{NO_3 Uptake}{NPP/S}$$

where S is Redfield C:N stoichiometry (106:16). We caution that while f_{is} is similar to the commonly used f-ratio (proportion of N uptake provided by NO₃⁻), it should not be interpreted as equivalent to the technical definition of the f-ratio (new production divided by total production), because we suspect that nitrification in the euphotic zone may have been significant (Kelly et al., in review; Stukel et al. this issue b). Furthermore, f_{is} may overestimate an f-ratio calculated from NO₃⁻ and NH₄⁺ uptake (see below), if phytoplankton engage in luxury nutrient uptake. With those caveats, vertically-integrated, cycle-average f_{is} ranged from 0.17-0.89; however, the high value (0.89 from C1), was heavily biased by the aforementioned high NO₃⁻ uptake outlier at the DCM. If the results from this day's experiments are excluded, f_{is} for this cycle decreases to 0.47. Across all cycles, f_{is} generally increased with depth in the euphotic zone. It is important to note that heterotrophic bacteria may play a role in nutrient uptake; however, the data suggests that

ammonium uptake was vertically-correlated with net primary production and phytoplankton growth rates (i.e., ammonium uptake was low at the light-limited DCM), while nitrate uptake was negligible during the night. Since community nitrate and ammonium uptake were light limited, we suspect that the majority of nutrient uptake was mediated by phytoplankton. Shipboard, depth-resolved NO₃ and NH₄ uptake experiments showed that NH₄ uptake is consistently higher than NO₃ uptake for all cycles and depths (Fig. 2). Similar to the findings from *in situ* experiments, the data suggests that NH₄⁺ is the preferred nitrogen source. Experiments during 2017 (mixed-layer only) showed little variability with depth, although NO₃⁻ uptake was higher in C1 than C2 (as suggested by f_{is}). NO₃⁻ and NH₄⁺ uptake rates from 2018 (which extended to the depth of the DCM) showed that NH₄⁺ uptake was lower at the DCM than in the mixed-layer, a finding that also agrees with our in situ NPP results. Shipboard incubationbased f-ratios ($f_{deck} = NO_3$ uptake / (NO_3 uptake + NH_4 uptake)) were lower than f_{is} and ranged from 0.02-0.17. For f_{deck} , we assumed that NH_4^+ uptake occurs at constant rates over the full 24h daily period (and hence multiplied 6-h experiments by 4), but that NO₃ uptake occurs only during the day (hence multiplied 6-h experiments by 2), based on the results of diel experiments (next section). Because f_{deck} calculated from NO₃⁻ and NH₄⁺ uptake measurements should be considered more accurate due to the shorter incubation times with less recycling occurring, we developed a blended f-ratio product: we treated f_{deck} as more accurate at paired depths, but used the vertical patterns from f_{is} . That is, we multiplied f_{is} by the ratio of f_{deck} : f_{is} at the nearest depths. This approach suggested that euphotic zone-averaged f-ratios varied from 0.02-0.22

331 332

(mean=0.06). f-ratios were slightly higher in the deep euphotic zone (>50 m depth, f ranged

from 0.03-0.44, mean=0.14) than in the shallow euphotic zone (f = 0.01-0.14, mean=0.06).

Diel variability in NPP and nutrient uptake

312

313

314

315

316

317

318

319

320

321

322

323

324

325

326

327

328

329

330

333

334

335

336

337

338

339

340

341

Distinct patterns emerged from the sequential 4-h incubations assessing diel variability in NH₄⁺ uptake (Fig. 3), NO₃⁻ uptake (Fig. 4), and NPP (Fig. 5). NO₃⁻ uptake and NPP were strongly light-dependent, with consistent mid-day peaks and low activity during the night (Figs. 4, 5). However, NH₄⁺ uptake showed no distinct diel patterns, with uptake rates as high at night as during the day. Comparison to simultaneous 24-h incubations allowed us to assess potential nutrient recycling in the euphotic zone. For NPP, the sum of six sequential 4-h H¹³CO₃⁻ uptake experiments were generally not significantly different from the mean of simultaneous 24-h

uptake experiments, indicating, as expected, that the time scale of H¹³CO₃⁻ recycling within the euphotic zone is long relative to the duration of a 24-h experiment. However, for both NO₃⁻ uptake and NH₄⁺ uptake rates, the sums of 4-h incubations were substantially greater than simultaneous 24-h incubations. For NO₃⁻ uptake, the ratio of the sum of sequential 4-h incubations to the average of 24-h incubations ranged from 1.2-5.6 (median=2.0). For NH₄⁺ uptake this ratio ranged from 5.0-6.0 (median=5.7). These results indicate rapid recycling of NH₄⁺ in the euphotic zone, and also reasonably fast recycling of NO₃⁻.

Vertical profiles of phytoplankton growth rates

Instantaneous growth rates of phytoplankton were variable as a function of depth and cycle (Fig. 6). On average, PRO surface growth rates were $0.67\pm0.35~d^{-1}$, decreasing with depth to $0.27\pm0.10~d^{-1}$ at the DCM. Similarly, the average SYN surface growth rates were $0.64\pm0.29~d^{-1}$, decreasing with depth to $0.34\pm0.30~d^{-1}$ at the DCM. These rates are consistent with previous research (Partensky *et al.*, 1999). DIAT growth, ranging from -0.4 to 1.5 d⁻¹, was higher in the upper euphotic zone and declined gradually with depth, except for a peak at 85 m during C4. ADINO growth ranged from 0-1.2 d⁻¹ and varied between cruises. In 2017 (C1-C3), growth of ADINOs was highest in the upper mixed-layer and gradually declined with depth. In 2018 experiments, (C4-C5), ADINO growth peaked in the mid euphotic zone at ~40 m. PRYM growth rate varied among cycles, ranging from -0.5 to 1.3 d⁻¹ with occasional peak values in the mid water column.

Model results

Using a Bayesian statistical approach to assimilate our *in situ* measurements, we constrained typical transfer functions used to model taxon-specific phytoplankton responses to light, temperature, and nutrient limitation in biogeochemical models. Data assimilation increased the fit to experimental data relative to the default parameterization from NEMURO-GoM (Supp. Fig. 2; Supp. Table I). The parameters determined from data assimilation had a much better fit to NPP observations than the default parameters, but only a moderately better fit to nitrate uptake observations (Fig. 7). The assimilated parameters underestimated observed nitrate uptake when nitrate uptake was high (although only by a factor of 2–5, while the default parameters underestimated nitrate uptake by ~10-fold). The model underestimate resulted from the fact that even with low half-saturation constants, the NEMURO model did not predict nitrate

372 uptake rates as high as the observations in a region with such low nitrate concentrations. Total 373 model log-likelihood increased substantially after the Bayesian optimization procedure 374 (from -40,748 to -3,333 for NEMURO-GOM default and data-assimilated parameters, 375 respectively, Supp. Table I). Notably, the default parameters predicted unrealistically low NPP 376 and growth rates for phytoplankton based on the low nutrient concentrations in the GoM 377 euphotic zone (Supp. Fig. 2). Consequently, the optimized parameter ranges suggested much 378 lower K_{NH4} (NH₄⁺ half-saturation constants) for all phytoplankton taxa except SYN (Fig. 8). 379 K_{NH4} was lowest for PRO (mean = 0.007 μ M, 95% C.I. = 0.005–0.009 μ M), which thrives in 380 oligotrophic regions. Previous research supports low half-saturation values for PRO (Marañón et 381 al., 2013; Grossowicz et al., 2017). In contrast, the posterior distributions for K_{NO3} remained 382 relatively close to the prior distributions (and to default NEMURO-GoM parameterizations, Fig. 8). The Bayesian parameter optimization approach suggested K_{NO3} values of ~ 3 µmol L^{-1} for all 383 384 large phytoplankton taxa, ~0.4 μmol L⁻¹ for PRO and OTHER, and ~0.1 μmol L⁻¹ for SYN. This 385 is comparable to laboratory studies that suggest half saturation constants are proportional to cell 386 size with larger cells ranging in value from 0.1-5.0 µmol L⁻¹ (Eppley et al., 1969). 387 Model results also varied among groups with respect to light-response parameters and 388 maximum growth rates. PRO and OTHER had the lowest maximum growth rates at 25°C (V_{25°C} = 0.82 d⁻¹, 95% C.I.=0.73-0.92 d⁻¹ and 0.44 d⁻¹, 95% C.I.=0.35-0.54 d⁻¹, respectively as shown in 389 390 Supplementary Fig. 2). However, the low maximum growth rate parameter suggested for 391 OTHER might be an artifact of the inclusion of many different taxa within this group, which 392 resulted in the model predicting low and only weakly-varying growth rates. All large 393 phytoplankton taxa had a maximum growth rate at 25°C of approximately 1.6-2.0 d⁻¹, while SYN had a higher maximum growth rate of 2.6-4.4 d^{-1} . PRO had the weakest light sensitivity, with α 394 395 (initial slope of the photosynthesis-irradiance relationship) equal to 0.01 m² W⁻¹ d⁻¹ (95%: 0.006-0.02 m² W⁻¹ d⁻¹), which likely reflects the presence of low-light-adapted PRO strains that thrive 396 397 in the deep euphotic zone. Most taxa had α in the range of 0.02-0.8 m² W⁻¹ d⁻¹ reflecting 398 substantial light limitation and reduced growth rates in the DCM (Fig. 8, Supp. Fig. 1).

Because we simultaneously varied all parameters, our optimization procedure provides some insight into correlations among parameters. A subset of these results (for PRO) are shown in Fig. 8. For instance, α and V were positively correlated suggesting that the model could fit

399

400

PRO growth rates at the DCM with either a higher maximum growth rate or with a weaker sensitivity to light limitation. Correlations for PRO were relatively weak for most parameter pairs. SYN, however, shows strong correlations for several parameter pairs. In particular, nutrient half-saturation constants were positively correlated with each other and with V. This suggests that the model could determine viable solution sets with high maximum growth rates and substantial nutrient limitation or with low maximum growth rates and weaker nutrient limitation, and that the relative importance of nutrient limitation by NO₃- or NH₄+ could vary (although K_{NO3} was always lower than K_{NH4} for SYN).

Comparison of optimized parameter sets to measured environmental conditions (nutrients, light, and temperature) also allowed us to assess patterns of limiting resources for each taxon (Fig. 9). While all phytoplankton taxa experienced slightly greater nutrient limitation in the shallow euphotic zone than in the deep euphotic zone, with the exception of SYN, nutrient limitation led to <50% decrease in growth rates (Fig. 9a). SYN was the only group with a median f-ratio greater than 0.05. This suggests that all taxa (except SYN) rely disproportionately on ammonium as a N source for growth and primary productivity. In contrast, SYN appeared to be the sole NO_3 specialist, with commensurately high f-ratios (<0.5) and greater nutrient limitation of growth rates. Our model thus shows a distinct niche specialization of the abundant taxa to the oligotrophic nature of this ecosystem.

With the exception of PRO and OTHER, which seem to be well-adapted to maintaining low and comparatively insensitive growth rates in both the mixed-layer and the deep euphotic zone, all taxa experienced substantial light limitation in the deep euphotic zone (>50 m). At these depths, light limitation ranged from mild limitation at ~50 m depth (e.g., growth penalties of ~20%) to strong limitation at the DCM (growth penalties of up to 95%). In comparison, no groups exhibited substantial light-limitation above 50 m; the greatest average light-limitation penalty in the upper 50 m was for DIAT (~10%), which had the highest photo-inhibition parameter.

DISCUSSION

Diel and vertical variability in phytoplankton productivity and nutrient utilization

Our data indicates that the oligotrophic GoM is a highly-stratified, picophytoplankton-

431 dominated (mostly PRO) region, with low nitrate concentrations (typically <0.1 µM above the DCM), low chlorophyll a concentrations (typically $<0.03 \text{ µg L}^{-1}$ in the mixed-layer and <0.2 µg432 433 L⁻¹ in the DCM), and deep DCMs (69 to 137 m). Nutrient uptake measurements show that NH₄⁺ 434 recycling is key to sustaining the phytoplankton community and productivity. These conclusions 435 are consistent with previous investigations of phytoplankton nutrient limitation in the oceanic 436 GoM (Dugdale and Goering, 1967; Eppley and Peterson, 1979; Platt and Harrison, 1985; 437 Lipschultz, 2001; Wawrik et al., 2004). 438 Vertical profiles of NPP (Fig. 1) and taxon-specific growth rates (Fig. 6) indicate that 439 phytoplankton and nutrient uptake are generally light limited, with NPP and growth rates 440 declining with depth. This decrease in NPP was not associated with a decline in phytoplankton 441 biomass. Although the biomass of different taxa varied with depth, overall phytoplankton 442 biomass and POC were typically relatively constant or increased slightly with depth (Selph et al., 443 this issue; Stukel et al., this issue a). This decrease in productivity and growth is more gradual, 444 however, than might be expected based on light limitation alone. Instead, it reflects substantial 445 nutrient limitation in surface waters that gradually gives way to light limitation in the deeper 446 euphotic zone, suggesting that phytoplankton throughout the euphotic zone grow at rates 447 substantially below their physiological potential. Vertical trends also likely include shifts in 448 species composition. Although these patterns are not evident from our FCM and HPLC-based 449 taxonomic study, sequencing data has shown differentially adapted species within our broad 450 categories, especially for high-light or low-light adapted PRO and SYN (Gutiérrez-Rodríguez et 451 al., 2016). Notably, the distinct DCM was primarily, but not solely, driven by increased cellular 452 pigmentation, as has been seen in multiple other studies (Cullen et al., 1982; Mignot et al., 453 2014). The maintenance of the DCM despite reduced growth rates thus requires either reduced 454 mortality (i.e., grazing) or subsidies from sinking phytoplankton (Hodges and Rudnick, 2004; 455 Moeller et al., 2019; Stukel et al., this issue a). 456 The diel experiments showed distinct temporal patterns of NH₄⁺ and NO₃⁻ uptake. NH₄⁺ 457 uptake rates did not vary with time of day (Fig. 3), while NO₃⁻ uptake rates were light-dependent 458 and similar to diel patterns of NPP (Figs. 4 and 5). This is consistent with NO₃- uptake being 459 more coupled to photosynthetic energy generation while NH₄⁺ uptake had no cellular regulation 460 (Figs. 3 and 4) (Dortch, 1990). Similar patterns have been found for NO₃- uptake in the Costa

Rica Dome (Stukel et al., 2016). However, NO₃ uptake rates measured in the Sargasso Sea were

lower at night but remained at $\sim 1/3$ daytime values (Lipschultz et al., 2001). In the Sargasso Sea, different studies have also given different ratios of daytime to nighttime NH₄⁺ uptake, with Lipschultz et al. (2001) determining that daytime rates were twice those of nighttime rates, while Glibert et al. (1988) found negligible day-night differences (as in our study). Lipschultz et al. (2001) methods included longer incubations (dusk to dawn) while Glibert et al. (1988) included short 1-2 h incubations. Taken together, these results underline the difficulty in extrapolating from short (2-6 h) experiments to daily uptake rates or f-ratios. Our diel uptake experiments also showed substantial differences between 4-h and 24-h NH₄⁺ uptake incubations (and to a lesser, but still considerable, extent for NO₃⁻ uptake incubations). Rapid cycling of NH₄⁺ in the surface ocean is expected, while NO₃ is often considered upwelled "new" nitrogen (Dugdale and Goering, 1967). Recent evidence, however, suggests that NO₃ regeneration through NH₄⁺ oxidation may be more common in surface oceans than previously realized (Yool et al., 2007, Shiozaki et al., 2016). The combination of relatively high rates of NO₃ uptake (compared to NO₃ concentration), very low NO₃ inventory from the surface to the DCM at ~100 m, and the ~2-fold higher NO₃ uptake measured in 4-h incubations relative to 24-h incubations lead us to believe that NO₃⁻ in the surface GoM might be supplied primarily by NH₄⁺ oxidation (Stukel et al., this issue b).

Model Optimization

462

463

464

465

466

467

468

469

470

471

472

473

474

475

476

477

478

479

480

481

482

483

484

485

486

487

488

489

490

491

492

Accurately constraining biogeochemical model parameters is a challenging yet crucial step towards treating models as falsifiable hypotheses (Arhonditsis and Brett, 2004; Anderson, 2005; Franks, 2009; Schartau *et al.*, 2017). Objective parameterization typically follows two broad approaches: (1) empirical fits of specific transfer functions to available data, or, (2) formal data assimilation. The former approach typically fits simple functional forms (e.g., photosynthesis-irradiance curves or Ivlev grazing formulations) to field or laboratory data. Empirical fits can be developed using experimental data derived from intentional manipulation of independent variables for a specific species or community (Eppley *et al.*, 1969; Platt *et al.*, 1980), or determined by fitting relationships for measurements made under natural conditions across an environmental gradient (Li *et al.*, 2010; Morrow *et al.*, 2018). These two empirical approaches address subtly different questions. The former approach examines the mechanistic response of a single taxon to changes in an environmental variable, while the latter addresses a

similar question but at a community-level scale, thus accounting for community shifts that occur with changes in light and nutrient conditions. This investigation of mechanistic responses at the community level is often more appropriate for models, because most such models simulate plankton functional groups comprised of many different species (Hood *et al.*, 2006). However, it is complicated by frequent covariance of multiple parameters (e.g., light and nutrients).

The alternative approach to model parameterization, which has long been common in physical oceanography, is formal data assimilation (Friedrichs *et al.*, 2006; Gregg *et al.*, 2009; Cummings *et al.*, 2013). In data assimilation, the full forward model is typically run and compared to observations, and then a prescriptive approach is followed to sequentially modify a subset of the parameters to minimize the model-data misfit. While multiple approaches have been used (Lawson *et al.*, 1995; Ward *et al.*, 2010; Doron *et al.*, 2011), the most common approach is the variational-adjoint, which is frequently used to compare model outputs to spatial maps of sea surface chlorophyll or time-series measurements of standing stocks in a one-dimensional framework. However, some studies have questioned whether assimilation of standing stock measurements is sufficient to constrain many model parameters, or have noted that more complex models often respond less well to assimilation techniques and the tendency of the variational-adjoint method to gravitate toward local minima in parameter space (Xiao and Friedrichs, 2014; Löptien and Dietze, 2015).

Our Bayesian statistical approach allows us to simultaneously constrain multiple parameters for which *a priori* estimates contained substantial uncertainty. The incorporation of multiple types of rate measurements allows for more precise determination of posterior distributions than would have been possible if we only utilized standing stock measurements. Indeed, optimized parameter values for the NEMURO-GoM transfer functions suggest >90% reduction in cost on average (Supp. Table I). The results returned reasonable parameter value ranges for most taxa, and demonstrated some expected emergent properties (e.g., PRO is an oligotrophic specialist). They also, however, disagreed with *a priori* expectations in some key ways, indicating that likelihood (i.e., our measurements) was more important than prior distributions in determining the posterior distributions. Most notably, the model showed that our experimental results could only be matched using much lower NH₄⁺ half-saturation values for

most taxa than the default values in NEMURO-GoM or common half-saturation constants measured in cultures (Edwards *et al.*, 2012; Shropshire *et al.*, 2020).

Nevertheless, some parameters seem unrealistic. Notably, the OTHER group, which is a composite of multiple phytoplankton taxa including pelagophytes, chlorophytes, prasinophytes, cryptophytes and other taxa, had very low maximum growth rates (mean: 0.44 d⁻¹, 95%: 0.35 – 0.54 d⁻¹ at 25°C) and very little nutrient or light limitation. This suggests that the optimization procedure attempted to give this composite group a low and relatively constant growth rate under all conditions. It is unlikely that pelagophytes, chlorophytes, prasinophytes, and cryptophytes were all insensitive to environmental variability. More likely, the different taxa within OTHERS have different responses to light and nutrients that are masked when they are aggregated together in a single group. On the other hand, this aggregate behavior might also be considered a strength of this parameterization approach, since even the most accurate representation of any one taxon or group can never reflect the adaptive physiological potential of a natural mixed community. It is also important to consider that groups like ADINO and OTHERS might be mixotrophic and taking up nitrogen by phagotrophy in this region, which may impact their functional responses to light and nutrient limitation (Jones 2000; Stoecker *et al.*, 2017).

Even though posterior distributions were very different from prior distributions, many of the parameters (e.g., K_{NH4}) retained substantial uncertainties. These uncertainties arise, in part, from covariance among environmental variables, which leads to correlations across the different parameters. In future work, experimental manipulations could be conducted in ways that break some of the natural correlations (e.g., nutrient amendments or light manipulation). In addition, some uncertainty undoubtedly arises from errors in measurements (nutrients, light, phytoplankton abundance). Future work could explicitly formulate the model such that the inputs are "true" values of standing stocks, defined as $X_i = \hat{X}_i + \delta_{Xi}$ for incubation i, where \hat{X}_i is the measured value and δ_{Xi} is a random variable with prior distribution centered at 0 and a standard deviation equal to the measurement uncertainty. The δ_{Xi} would then be variables to solve for parameter solutions. Even without these potential improvements, however, we believe that our approach provides useful guidance for parameterizing future biogeochemical models of the GoM and elsewhere.

Phytoplankton niches in the oligotrophic ocean

552

553

554

555

556

557

558

559

560

561

562

563

564

565

566

567

568

569

570

571

572

573

574

575

576

577

578

579

580

581

The vast number of species, strains, or ecotypes that are aggregated into our broad phytoplankton taxonomic groups make it difficult to define specific niches for each group (Scanlan, 2003; Simon *et al.*, 2009; Kashtan *et al.*, 2014). It is reasonable to expect that the evolutionary history of taxa provides some inherited physiological constraints on their overall niche space, while the prevalence of specific ecotypes may contribute further to a definable niche space for each group. Our results, with respect to both spatial patterns of abundance and model constrained characteristics, shed light on these questions.

The two cyanobacterial taxa have distinctly different ecological niches. For PRO, the consistent subsurface maxima just above the DCM (Selph et al., this issue) and high α (initial slope of the photosynthesis-irradiance curve) indicates that it thrives in low-light conditions. We also observed a substantial increase in divinyl chlorophyll a cell-1 with depth that likely explains its physiological adaptation to low light (whether by cellular regulation or distinct ecotypes remains unconstrained). Other studies have shown that there are distinct depth distributions of PRO ecotypes (HLI and HLII near the surface, and LL at low light) (Zwirglmaier et al., 2007). Beyond light limitation, the very low NH₄⁺ half-saturation constant shows it to be a low-nutrient specialist that relies almost exclusively on rapidly recycled NH₄⁺. This concurs with a general consensus that although some strains of PRO contain genes for NO₃⁻ assimilation (Martiny et al., 2009), this genus primarily utilizes NH₄⁺ (Moore *et al.*, 2002). In contrast, SYN was the only group that efficiently exploited low nitrate concentrations, typically maintaining a shallower distribution in the water column with greater sensitivity to light limitation. We thus suspect that SYN relies substantially on NO₃ regenerated in the upper euphotic zone through shallow nitrification (Kelly et al., submitted; Stukel et al., this issue b). Previous research has shown similar fundamental differences between SYN and PRO in nutrient utilization, with SYN utilizing nitrate more efficiently than PRO (Scanlan and West, 2002). Comparisons of abundances to nutrient concentrations and turbulent mixing rates have also suggested that PRO is more abundant in warm waters with low nitrate supply, while SYN and picoeukaryote niches are in cooler waters with greater nitrate supply (Otero-Ferrer et al., 2018), a finding that agrees with previous evidence showing PRO dominance in oligotrophic gyres and SYN and picoeukaryotes becoming more important in equatorial upwelling and temperate regions (Zubkov et al., 2000; Landry and Kirchman, 2002).

Model results for eukaryotic phytoplankton taxa were slightly less conclusive. The larger uncertainty is partially due to the substantially lower abundance of these taxa, and also in part because the pigment-based growth rates were imperfect estimates of true cellular growth of these taxa. DIAT had modest maximum growth rates, lower than those in many culture and field measurements (e.g., Furnas, 1990; Sarthou et al., 2005; Selph et al., 2011; Selph et al., 2016). This might, however, reflect chronic extreme silicon limitation, which was not assessed in our study. We do note that prior concentration measurements from GoM indicate that Si is very low (Dortch and Whitledge, 1992). Irwin et al. (2012) used continuous-plankton-recorder-derived phytoplankton abundance data to show that diatoms and dinoflagellates have distinct ecological niches with diatoms typically excelling in cold, nutrient-rich, well-mixed, low-light environments relative to dinoflagellates, which agrees with the low diatom biomasses we found. Barton et al. (2015) further showed that diatom responses to these physical drivers are spatiotemporally variable, which does suggest caution when applying our results to other regions. Our model could not significantly differentiate between ADINO and PRYMN, both of which had maximum growth rates of ~0.6 d⁻¹ and exhibited substantial light limitation. The model did, however, suggest that the NH₄⁺ half-saturation constant was substantially lower for PRYMN than ADINO, which is not surprising for a generally smaller phytoplankton taxon and might help explain why PRYM was the biomass-dominant eukaryote in our study (Selph et al., this issue). Considered together, these results delineate distinct competitive differences between these diverse phytoplankton functional groups, which helps explain their coexistence in oligotrophic conditions and supports the advanced light and nutrient resource competition model (Burson et al 2018).

CONCLUSION

582

583

584

585

586

587

588

589

590

591

592

593

594

595

596

597

598

599

600

601

602

603

604

605

606

607

608

609

610

611

The oceanic GoM is an extremely oligotrophic ecosystem with low NPP and a strong DCM. We found higher NPP in the upper euphotic zone than the DCM, fueled mostly by recycled nutrients. Ammonium uptake exceeded nitrate uptake at all depths and was relatively invariant with time of day, while nitrate uptake was mainly restricted to daytime. Bayesian parameter optimization techniques allowed us to constrain maximum growth rates, light utilization parameters, and half saturation constants for five phytoplankton taxa (PRO, SYN, DIAT, PRYMN and ADINO), yielding parameter values for future modeling studies. This

612 approach also allowed us to define distinct niches for different taxa and determine that all, except 613 PRO, were chronically nutrient limited at all depths. 614 **ACKNOWLEDGEMENTS** 615 This manuscript would not have been possible without the support from the captain, crew and 616 research technicians aboard the NOAA Ship Nancy Foster; thank you for your dedication and 617 hard work. In addition, we would like to acknowledge and thank our collaborators at NOAA 618 Southeast Fisheries/RASMAS/University of Miami for their effort and perseverance on leading 619 two successful cruises. 620 **FUNDING** 621 This study acknowledges BLOOFINZ-GoM Program support from the National Oceanic and 622 Atmospheric Administration's RESTORE Program Grant (Project Title: Effects of nitrogen 623 sources and plankton food-web dynamics on habitat quality for the larvae of Atlantic bluefin 624 tuna in the Gulf of Mexico) under federal funding opportunity NOAA-NOS-NCCOS-2017-625 2004875, including NOAA JIMAR Cooperative Agreement, award #NA16NMF4320058, 626 NOAA CIMAS Cooperative Agreement, award #NA15OAR4320064, and NOAA CIMEAS 627 Cooperative Agreement, and U.S. National Science Foundation grant OCE -1851558. 628 **DATA ARCHIVING** 629 Data presented here have been submitted to the National Oceanic and Atmospheric 630 Administration's (NOAA) National Centers for Environmental Information (NCEI) data 631 repository and will also be archived at BCO-DMO (Biological and Chemical Oceanography Data 632 Management Office) site https://www.bco-dmo.org/program/819631. Model code and dataset 633 are freely available on Github (https://github.com/tbrycekelly/Yingling/) with instructions on 634 how to replicate model results. 635 636 **REFERENCES** 637 Anderson, T. R. (2005) Plankton functional type modelling: running before we can walk? J. 638 Plankton Res., 27, 1073-1081.

- Arhonditsis, G. B. and Brett, M. T. (2004) Evaluation of the current state of mechanistic aquatic
- biogeochemical modeling. *Mar. Ecol. Prog. Ser.*, **271**, 13-26.
- Barton, A. D., Lozier, M. S. and Williams, R. G. (2015) Physical controls of variability in North
- Atlantic phytoplankton communities. *Limnol. Oceanogr.*, **60**, 181-197.
- Bertilsson, S., Berglund, O., Karl, D. M. and Chisholm, S. W. (2003) Elemental composition of
- marine *Prochlorococcus* and *Synechococcus*: Implications for the ecological stoichiometry of
- the sea. *Limnol. Oceanogr.*, **48**, 1721-1731.
- Biggs, D. C. (1992) Nutrients, plankton, and productivity in a warm-core ring in the western
- 647 Gulf of Mexico. *J. Geophys. Res: Oceans.*, **97**, 2143-2154.
- Biggs, D. C., Hu, C. and Müller-Karger, F. E. (2008) Remotely sensed sea-surface chlorophyll
- and POC flux at Deep Gulf of Mexico Benthos sampling stations. *Deep-Sea Res. II*, **55**,
- 650 2555-2562.
- Biggs, D. C. and P. H. Ressler. (2001) Distribution and abundance of phytoplankton,
- zooplankton, ichthyoplankton, and micronekton in the deepwater Gulf of Mexico. *Gulf of*
- 653 *Mex. Sci.*, **19**, 1-23.
- Bouman, H. A., Platt, T., Doblin, M., Figueiras, F. G., Gudmundsson, K., Gudfinnsson, H. G.,
- Huang, H. G., Hickman, B., et al. (2018) Photosynthesis–irradiance parameters of marine
- phytoplankton: synthesis of a global data set. Earth Sys. Sci. Data, 10, 251-266.
- 657 Brown, S. L., Landry, M. R., Selph, K. E., Yang, E. J., Rii, Y. M. and Bidigare, R. R. (2008)
- Diatoms in the desert: Plankton community response to a mesoscale eddy in the subtropical
- North Pacific. *Deep-Sea Res. II*, **55**, 1321-1333.
- Burson, A., Stomp, M., Greenwell, E., Grosse, J. and Huisman, J. (2018) Competition for
- nutrients and light: testing advances in resource competition with a natural phytoplankton
- 662 community. *Ecology*, **99**, 1108-1118.
- 663 Chisholm, S. W., Olson, R. J., Zettler, E. R., Goericke, R., Waterbury, J. B. and Welschmeyer,
- N. A. (1988) A novel free-living prochlorophyte abundant in the oceanic euphotic zone.
- 665 *Nature*, **334**, 340-343.
- 666 Cornic, M., Smith, B. L., Kitchens, L. L., Bremer, J. R. A. and Rooker, J. R. (2018) Abundance
- and habitat associations of tuna larvae in the surface water of the Gulf of Mexico.
- 668 *Hydrobiologia*, **806**, 29-46.

- 669 Cullen, J. J. (1982) The deep chlorophyll maximum: comparing vertical profiles of chlorophyll a.
- 670 Can. J. Fish. Aquat. Sci., **39**, 791-803.
- 671 Cummings, J. A. and Smedstad, O. M. (2013) Variational data assimilation for the global ocean.
- Data Assimilation for Atmospheric, Oceanic and Hydrologic Applications. 303-343.
- Davey, M., Tarran, G. A., Mills, M. M., Ridame, C., Geider, R. J. and Laroche, J. (2008)
- Nutrient limitation of picophytoplankton photosynthesis and growth in the tropical North
- 675 Atlantic. *Limnol. Oceanogr.*, **53**, 1722-1733.
- De Martini, F., Neuer, S., Hamill, D., Robidart, J. and Lomas, M. W. (2018) Clade and strain
- specific contributions of Synechococcus and Prochlorococcus to carbon export in the
- 678 Sargasso Sea. *Limnol. Oceanogr.*, **63**, 448-457.
- Doron, M., Brasseur, P. and Brankart, J. M. (2011) Stochastic estimation of biogeochemical
- parameters of a 3D ocean coupled physical-biogeochemical model: Twin experiments. J. of
- 681 *Mar. Sys.*, **87**, 194-207.
- Dortch, Q. (1990) The interaction between ammonium and nitrate uptake in phytoplankton. Mar.
- 683 Ecol. Prog. Ser., **61**, 183-201.
- Dortch, Q. and Whitledge, T. E. (1992) Does nitrogen or silicon limit phytoplankton production
- in the Mississippi River plume and nearby regions? *Cont. Shelf Res.*, **12**, 1293-1309.
- Duce, R. A., LaRoche, J., Altieri, K., Arrigo, K. R., Baker, A. R., Capone, D. G., Cornell, S.,
- Dentener, F., et al. (2008) Impacts of atmospheric anthropogenic nitrogen on the open
- 688 ocean. Science, **320**, 893-897.
- Dugdale, R. C. and Goering, J. J. (1967) Uptake of New and Regenerated Forms of Nitrogen in
- 690 Primary Productivity. *Limnol. Oceanogr.*, **12**, 196-206.
- Dugdale, R. C. and Wilkerson, F. P. (1986) The use of 15N to measure nitrogen uptake in
- 692 eutrophic: experimental considerations. *Limnol. Oceanogr.*, **31**, 673-689.
- Dutkiewicz, S., Scott, J. R. and Follows, M. J. (2013) Winners and losers: Ecological and
- biogeochemical changes in a warming ocean. *Global Biogeochem. Cycles*, **27**, 463-477.
- 695 Edwards, K. F., Thomas, M. K., Klausmeier, C. A. and Litchman, E. (2012) Allometric scaling
- and taxonomic variation in nutrient utilization traits and maximum growth rate of
- 697 phytoplankton. *Limnol. Oceanogr.*, **57**, 554-566.
- 698 Eppley, R. W. and Peterson, B. J. (1979) Particulate organic matter flux and planktonic new
- production in the deep ocean. *Nature*, **282**, 677-680.

- 700 Eppley, R. W., Rogers, J. N. and McCarthy, J. J. (1969) Half-saturation constants for uptake of
- 701 nitrate and ammonium by marine phytoplankton. *Limnol. Oceanogr.*, **14**, 912-920.
- Fennel, K., Wilkin, J., Levin, J., Moisan, J., O'Reilly, J. and Haidvogel, D. (2006) Nitrogen
- cycling in the Middle Atlantic Bight: Results from a three-dimensional model and
- implications for the North Atlantic nitrogen budget. *Glob. Biogeochem. Cycles*, 20.
- Follows, M. J. and Dutkiewicz, S. (2011) Modeling diverse communities of marine
- 706 microbes. Ann, Rev. Mar. Sci., 3, 427-451.
- Forristall, G. Z., Schaudt, K. J. and Cooper, C. K. (1992) Evolution and kinematics of a Loop
- Current eddy in the Gulf of Mexico during 1985. J. Geophys. Res.: Oceans, 97, 2173-2184.
- 709 Franks, P. J. (2009). Planktonic ecosystem models: perplexing parameterizations and a failure to
- 710 fail. J. Plankton Res., **31**, 1299-1306.
- Friedrichs, M. A. M., Hood, R. R. and Wiggert, J. D. (2006) Ecosystem model complexity versus
- 712 physical forcing: Quantification of their relative impact with assimilated Arabian Sea data.
- 713 *Deep-Sea Res. II*, **53**, 576-600.
- Furnas, M. J. (1990) *In situ* growth rates of marine phytoplankton: approaches to measurement,
- 715 community and species growth rates. J. Plankton Res., 12, 1117-1151.
- Garrison, D. L., Gowing, M. M., Hughes, M. P., Campbell, L., Caron, D. A., Dennett, M. R.,
- Shalapyonok, A., Olson, R. et al. (2000) Microbial food web structure in the Arabian Sea: a
- 718 US JGOFS study. *Deep-Sea Res. II*, **47**, 1387-1422.
- Gerard, T., Lamkin, J. T., Kelly, T. B., Knapp, A. N., Laiz-Carrión, R., Malca, E., Selph, K. E.,
- Shiroza, A. et al.. (this issue) Bluefin Larvae in Oligotrophic Ocean Foodwebs,
- Investigations of Nutrients to Zooplankton: Overview of the BLOOFINZ-Gulf of Mexico
- 722 program. J. Plankton Res.
- Glibert. P. M., Dennett, M.R. and Caron, D. A. (1988) Nitrogen uptake and NH4+ regeneration
- by pelagic microplankton and marine snow from the North Atlantic. J. Mar. Res, 46, 837-
- 725 852.
- Gomez, F. A., Lee, S.-K., Liu, Y., Hernandez Jr, F. J., Müller-Karger, F. E. and Lamkin, J. T.
- 727 (2018) Seasonal patterns in phytoplankton biomass across the northern and deep Gulf of
- Mexico: a numerical model study. *Biogeo.*, **15**, 3561-3576.

- Gregg, W. W., Friedrichs, M. A., Robinson, A. R., Rose, K. A., Schlitzer, R., Thompson, K. R.
- and Doney, S. C. (2009) Skill assessment in ocean biological data assimilation. *J. Mar.*
- 731 *Sys.*, **76**(1-2), 16-33.
- Grossowicz, M., Roth-Rosenberg, D., Aharonovich, D., Silverman, J., Follows, M. J. and Sher,
- D. (2017) *Prochlorococcus* in the lab and *in silico*: The importance of representing
- 734 exudation. *Limnol. Oceanogr.*, **62**, 818-835.
- Gutiérrez-Rodríguez, A., Selph, K. E. and Landry, M. R. (2016) Phytoplankton growth and
- microzooplankton grazing dynamics across vertical environmental gradients determined by
- transplant in situ dilution experiments. J. Plankton Res., 38, 271-289.
- Hastings, W. K. (1970) Monte Carlo sampling methods using Markov chains and their
- 739 applications. *Biometrika*, **57**, 97-109.
- Higgins, H., Wright, S. and Schlüter, L. (2011) Quantitative interpretation of chemotaxonomic
- pigment data. In Roy, S., Llewellyn, C., Egeland, E., and Johnsen, G. (eds.), *Phytoplankton*
- Pigments: Characterization, Chemotaxonomy and Applications in Oceanography,
- Cambridge University Press, Cambridge, 257-313.
- Hodges, B. A. and Rudnick, D. L. (2004) Simple models of steady deep maxima in chlorophyll
- and biomass. *Deep Sea Res.: Part 1*, **51**, 999-1015.
- Hood, R. R., Laws, E. A., Armstrong, R. A., Bates, N. R., Brown, C. W., Carlson, C. A., Chai,
- F., Doney, S. C., et al. (2006) Pelagic functional group modeling: Progress, challenges and
- 748 prospects. *Deep-Sea Res. II*, **53**, 459-512.
- 1749 Irwin, A. J., Nelles, A. M. and Finkel, Z. V. (2012) Phytoplankton niches estimated from field
- 750 data. *Limnol. Oceanogr.*, **57**, 787-797.
- Jones, R. I. (2000) Mixotrophy in planktonic protists: an overview. Freshwater Biol., 45, 219-
- 752 226.
- Kashtan, N., Roggensack, S. E., Rodrigue, S., Thompson, J. W., Biller, S. J., Coe, A., Ding, H.,
- 754 Marttinen, P., et al. (2014) Single-cell genomics reveals hundreds of coexisting
- subpopulations in wild *Prochlorococcus*. *Science*, **344**, 416-420.
- 756 Kelly, T. B., Knapp, A. N., Landry, M. R., Selph, K. E., Shropshire, T. A., Thomas, R. and
- 757 Stukel, M. R. (in review) Lateral advection supports nitrogen export in the oligotrophic open-
- ocean Gulf of Mexico. *Nature Comm.*

- Kent, A. G., Dupont, C. L., Yooseph, S. and Martiny, A. C. (2016) Global biogeography of
- 760 *Prochlorococcus* genome diversity in the surface ocean. *ISME J*, **10**, 1856-1865.
- Knapp, A. N., Thomas, R., Stukel, M. R., Kelly, T. B., Landry, M. R., Selph, K. E., Malca, E.,
- Gerard, T., et al. (this issue) Constraining the sources of nitrogen fueling phytoplankton and
- food webs in the Gulf of Mexico using nitrogen isotope budgets. J. Plankton Res.
- Landry, M. R., Brown, S. L., Rii, Y. M., Selph, K. E., Bidigare, R. R., Yang, E. J. and Simmons,
- M. P. (2008) Depth-stratified phytoplankton dynamics in Cyclone *Opal*, a subtropical
- 766 mesoscale eddy. *Deep-Sea Res. II*, **55**, 1348-1359.
- Landry, M. R., Haas, L. W. and Fagerness, V. L. (1984) Dynamics of microbial plankton
- 768 communities: experiments in Kaneohe Bay, Hawaii. Mar. Eco. Pro. Series, 16, 127-133.
- Landry, M. R., and R. P. Hassett. (1982) Estimating the grazing impact of marine
- 770 microzooplankton. *Mar. Bio.*, **67**, 283-288.
- Landry, M. R. and D. L. Kirchman. (2002) Microbial community structure and variability in the
- 772 tropical Pacific. *Deep-Sea Res. II*, **49**, 2669-2694.
- Landry, M. R., Ohman, M. D., Goericke, R., Stukel, M. R. and Tsyrklevich, K. (2009)
- Lagrangian studies of phytoplankton growth and grazing relationships in a coastal upwelling
- ecosystem off Southern California. *Prog. Oceanogr.*, **83**, 208-216.
- Landry, M. R., Selph, K. E., Stukel, M. R., Swalethorp, R., Kelly, T. B., Beatty, J. and
- Ouackenbush, C. (this issue) Microbial food web dynamics in the oceanic Gulf of Mexico. J.
- 778 Plankton Res.
- Landry, M. R., Selph, K. E. and Yang, E.-J. (2011) Decoupled phytoplankton growth and
- microzooplankton grazing in the deep euphotic zone of the HNLC equatorial Pacific. *Mar*.
- 781 *Ecol. Prog. Ser.* **421**: 13-24.
- Lawson, L. M., Spitz, Y. H., Hofmann E. E. and Long, R. B. (1995) A Data Assimilation
- Technique Applied to a Predator-Prey Model. *Bull. Math. Bio.*, **57**, 593-617.
- Li, Q. P., Franks, P. J., Landry, M. R., Goericke, R. and Taylor, A. G. (2010) Modeling
- phytoplankton growth rates and chlorophyll to carbon ratios in California coastal and pelagic
- 786 ecosystems. J. Geophys. Res.: Biogeosci., 115, 1-12.
- Li, J., Plouchart, D., Zastepa, A. and Dittrich, M. (2019) Picoplankton accumulate and recycle
- 788 polyphosphate to support high primary productivity in coastal Lake Ontario. Sci. Reports, 9,
- 789 1-10.

- 790 Lipschultz, F. (2001) A time-series assessment of the nitrogen cycle at BATS. *Deep-Sea Res. II*,
- 791 **48**, 1897-1924.
- Löptien, U., and Dietze, H. (2015) Constraining parameters in marine pelagic ecosystem
- models—is it actually feasible with typical observations of standing stocks? *Ocean Science*,
- 794 **11**, 573-590.
- 795 Marañón, E., Cermeño, P., López-Sandoval, D. C., Rodríguez-Ramos, T., Sobrino, C., Huete-
- Ortega, M., Blanco, J. M., Rodríguez, J. (2013) Unimodal size scaling of phytoplankton
- 797 growth and the size dependence of nutrient uptake and use. *Eco. letters*, **16**, 371-379.
- Martiny, A. C., Kathuria, S. and Berube, P. M. (2009) Widespread metabolic potential for nitrite
- and nitrate assimilation among Prochlorococcus ecotypes. *Proc. Natl. Acad. Sci.*, **106**, 10787-
- 800 10792.
- 801 Menden-Deuer, S. and Lessard, E. J. (2000) Carbon to volume relationships for dinoflagellates,
- diatoms, and other protist plankton. *Limnol. Oceanogr.*, **45**, 569-579.
- Mignot, A., Claustre, H., Uitz, J., Poteau, A., d'Ortenzio, F. and Xing, X. (2014). Understanding
- the seasonal dynamics of phytoplankton biomass and the deep chlorophyll maximum in
- oligotrophic environments: A Bio-Argo float investigation. Global Biogeochem. Cycles, 28,
- 806 856-876.
- Moeller, H. V., Laufkötter, C., Sweeney, E. M. and Johnson, M. D. (2019) Light-dependent
- grazing can drive formation and deepening of deep chlorophyll maxima. *Nat. Commun.*, 10,
- 809 1-8.
- Moisan, T. A., Blattner, K. L. and Makinen, C. P. (2010) Influences of temperature and nutrients
- on Synechococcus abundance and biomass in the southern Mid-Atlantic Bight. Contin. Shelf
- 812 *Res.*, **30**, 1275-1282.
- Monger, B. C. and Landry, M. R. (1993) Flow cytometric analysis of marine bacteria with 729
- 814 Hoechst 33342. *Appl. Environ. Microbiol.*, **59**, 905-911.
- Monterey, G., and Levitus, S. (1997) Seasonal Variability of Mixed Layer Depths for the World,
- NOAA Atlas NESDIS 14. Washington, DC: US Government Printing Office.
- Moore, L.R., Post, A. F., Rocap, G. and Chisholm, S. W. (2002) Utilization of different nitrogen
- sources by the marine cyanobacteria *Prochlorococcus* and *Synechococcus*. *Limnol*.
- 819 *Oceanogr.*, **47**, 989–996.

- Moore, L.R., Rocap, G. and Chisholm, S. W. (1998) Physiology and molecular phylogeny of
- coexisting *Prochlorococcus* ecotypes. *Nature*, **393**, 464–467.
- Morrow, R., Goericke, R., Kelly, T. B., Landry, M. R., Ohman, M. D., Stephens, B. M. and
- Stukel, M. R. (2018) Primary productivity, mesozooplankton grazing, and the biological
- pump in the California Current Ecosystem: Variability and response to El Niño. *Deep-Sea*
- 825 Res. I, **140**, 52-62.
- Mulholland, M. R. and Lomas, M. W. (2008) Nitrogen uptake and assimilation. *Nitrogen Mar*.
- 827 Environ. 303-384.
- 828 Oey, L., Ezer, T. and Lee, H. (2005) Loop Current, rings and related circulation in the Gulf of
- Mexico: A review of numerical models and future challenges. Geo. Monograph-American
- 830 Geo. Union, **161**, 31.
- Partensky, F., Hess, W. R. and Vaulot, D. (1999) *Prochlorococcus*, a marine photosynthetic
- prokaryote of global significance. *Microbiol. Mol. Biol. Rev.*, **63**, 106-127.
- Platt, T. G. C. L., Gallegos, C. L. and Harrison, W. G. (1980) Photoinhibition of photosynthesis
- in natural assemblages of marine phytoplankton. J. Mar. Res, **38**(4), 687-701.
- Platt, T., and Harrison, W. G. (1985) Biogenic fluxes of carbon and oxygen in the ocean. *Nature*,
- **318**, 55-58.
- Redfield, A. C., Ketchum, B. H., and Richards, F. A. (1963). The influence of organisms on the
- composition of sea water, in The Sea. *Interscience*, **2**, 26-77.
- Rocap, G., Larimer, F. W., Lamerdin, J., Malfatti, S., Chain, P., Ahlgren, N. A., Arellano, A.,
- Coleman, M., et al. (2003) Genome divergence in two *Prochlorococcus* ecotypes reflects
- oceanic niche differentiation. *Nature*, **424**, 1042-1047.
- Rooker, J. R., Bremer, J. R. A., Block, B. A., Dewar, H., De Metrio, G., Corriero, A., Kraus, R.
- T., Prince, et al. (2007) Life history and stock structure of Atlantic bluefin tuna (*Thunnus*
- 844 *thynnus*). Rev. in Fish. Sci., **15**, 265-310.
- 845 Sarthou, G., Timmermans, K. R., Blain, S. and Tréguer, P. (2005) Growth physiology and fate of
- diatoms in the ocean: a review. J. Sea Res., 53, 25-42.
- Scanlan, D. J. and West, N. J. (2002) Molecular ecology of the marine cyanobacterial genera
- 848 Prochlorococcus and Synechococcus. FEMS Microbiol. Ecol, 40, 1-12.

- Schartau, M., Wallhead, P., Hemmings, J., Löptien, U., Kriest, I., Krishna, S., Ward, B. A.,
- Slawig, T., et al. (2017) Reviews and syntheses: parameter identification in marine
- planktonic ecosystem modelling. *Biogeo.*, **14**, 1647-1701.
- 852 Selph, K. E., Landry, M. R., Taylor, A. G., Gutierrez-Rodriguez, A., Stukel, M. R., Wokuluk, J.
- and Pasulka, A. (2016) Phytoplankton production and taxon-specific growth rates in the
- 854 Costa Rica Dome. *J. Plankton Res.*, **38**, 199-215.
- 855 Selph, K. E., Landry, M. R., Taylor, A. G., Yang, E. J., Measures, C. I., Yang, J., Stukel, M. R.,
- Christensen, S., et al. (2011) Spatially-resolved taxon-specific phytoplankton production and
- grazing dynamics in relation to iron distributions in the Equatorial Pacific between 110 and
- 858 140°W. Deep-Sea Res. II, **58**, 358-377.
- 859 Selph, K. E., Shacat, J. and Landry, M. R. (2005) Microbial community composition and growth
- rates in the NW Pacific during spring 2002. Geochem. Geophys. Geosys., 6, doi.org/
- 861 10.1029/2005GC000983
- 862 Selph, K. E., Swalethorp, R., Stukel, M. R., Kelly, T. B., Knapp, A. N., Fleming, K., Hernandez,
- T. and Landry, M. R. (this issue) <u>Phytoplankton community composition and biomass in the</u>
- 864 <u>oligotrophic Gulf of Mexico</u>. *J. Plankton Res*.
- Sherr, E. B., Caron, D. A. and Sherr, B. F. (1993) Staining of heterotrophic protists for
- visualization via epifluorescence microscopy. Handbook of methods in aquatic microbial
- 867 *ecology*, 213-227.
- 868 Sherr, B. F. and E. B. Sherr (1993) Preservation and storage of samples for enumeration of
- heterotrophic protists. In Kemp, P. F., Sherr, B. F., Sherr, E. B. and Cole, J. J. (eds.) *Handbook*
- of Methods in Aquatic Microbial Ecology. CRC Press, pp. 207-212.
- 871 Shiozaki, T., Ijichi, M., Isobe, K., Hashihama, F., Nakamura, K. I., Ehama, M., Hayashizaki, K.,
- Takahashi, K. et al. (2016). Nitrification and its influence on biogeochemical cycles from the
- equatorial Pacific to the Arctic Ocean. *The ISME journal*, **10**, 2184-2197.
- 874 Shropshire, T. A., Morey, S. L., Chassignet, E. P., Bozec, A., Coles, V. J., Landry, M. R.,
- Swalethorp, R., Zapfe, G. et al. (2020) Quantifying spatiotemporal variability in zooplankton
- dynamics in the Gulf of Mexico with a physical-biogeochemical model. *Biogeosci.*, 17,
- 877 3385-3407.
- 878 Shropshire, T. A., Morey, S. L., Chassignet, E. P., Karnauskas, M., Coles, V. J., Malca, E., Laiz-
- Carrión, R., Fiksen, O., Shiroza, A., Quintanilla Hervas J. M., Gerard, T., Lamkin, J. T., and

- Stukel, M. R., (this issue) Trade-offs between risks of predation and starvation in larvae
- make the shelf break an optimal spawning location for Atlantic Bluefin tuna. *J. Plankton Res.*
- 883 Simon, N., Cras, A. L., Foulon, E. and Lemee, R. (2009) Diversity and evolution of marine
- phytoplankton. C. R. Biol., **332**, 159-170.

- Stoecker, D.K. (1999) Mixotrophy among dinoflagellates. J. Euk. Microbiol., 46, 397–401.
- Stoecker, D. K., Hansen, P. J., Caron, D. A. and Mitra, A. (2017) Mixotrophy in the marine
- 887 plankton. Annu. Rev. Mar. Sci., 9, 311-335.
- 888 Strom, S. L. and Morello, T. A. (1998) Comparative growth rates and yields of ciliates and
- heterotrophic dinoflagellates. *J. Plankton Res.*, **20**, 571-584.
- 890 Strickland, J. D. H. and Parsons, T. R. (1972) A practical handbook of seawater analysis. Bull.
- 891 Fish. Res. Board Can., **167**, 1-130.
- 892 Stukel, M. R. (2020) Investigating equations for measuring dissolved inorganic nutrient uptake
- in oligotrophic conditions. *BioRxiv*, 2020.08.30.274449.
- Stukel, M. R., Benitez-Nelson, C. R., Decima, M., Taylor, A. G., Buchwald, C. and Landry, M.
- R. (2016) The biological pump in the Costa Rica Dome: an open-ocean upwelling system
- with high new production and low export. *J. Plankton Res.*, **38**, 348–365.
- Stukel, M. R., Gerard, T., Kelly, T. B., Knapp, A. N., Laiz-Carrion, R., Lamkin, J. T., Landry,
- M. R., Malca, E., et al. (this issue b) Plankton food webs of the Gulf of Mexico spawning
- grounds of Atlantic Bluefin tuna. J. Plankton Res.
- 900 Stukel, M. R., Kelly, T. B., Landry, M. R., Selph, K. E. and Swalethorp, R. (this issue a) Sinking
- carbon, nitrogen, and pigment flux within and beneath the euphotic zone in the oligotrophic,
- open-ocean Gulf of Mexico. J. Plankton Res.
- 903 Stukel, M. R., Kahru, M., Benitez-Nelson, C. R., Decima, M., Goericke, R., Landry, M. R. and
- Ohman, M. D. (2015) Using Lagrangian-based process studies to test satellite algorithms of
- vertical carbon flux in the eastern North Pacific Ocean. J. Geophys. Res.: Oceans, 120, 7208-
- 906 7222.
- Walker, N. D., Leben, R. R. and Balasubramanian, S. (2005) Hurricane-forced upwelling and
- chlorophyll a enhancement within cold-core cyclones in the Gulf of Mexico. Geo. Res.
- 909 *Letters*, **32**.

- 910 Ward, B. A., Friedrichs, M. A. M., Anderson T. R. and Oschlies, A. (2010) Parameter
- optimisation techniques and the problem of underdetermination in marine biogeochemical
- 912 models. J. Mar. Sys., **81**, 34-43.
- Wawrik, B., Paul, J. H., Bronk, D. A., John, D. and Gray, M. (2004) High rates of ammonium
- recycling drive phytoplankton productivity in the offshore Mississippi River plume. *Aquat*.
- 915 *Microb. Ecol.*, **35**, 175-184.
- Wright, S. (2008) Chemtax version 1.95 for calculating the taxonomic composition of
- 917 phytoplankton populations, Ver. 1, Australian Antarctic Data Centre, doi:
- 918 10.4225/15/59fff1c5ea8fc, Accessed: 2020-06-01.
- Yiao, Y. and Friedrichs, M. A. M. (2014) Using biogeochemical data assimilation to assess the
- relative skill of multiple ecosystem models in the Mid-Atlantic Bight: effects of increasing
- the complexity of the planktonic food web. *Biogeo.*, **11**, 3015-3030.
- 922 Yool, A., Martin, A. P., Fernández, C. and Clark, D. R. (2007) The significance of nitrification
- for oceanic new production. *Nature*, **447**, 999-1002.
- 24 Zubkov, M. V., Sleigh, M. A., Burkill, P. H. and Leakey, R. J. (2000) Picoplankton community
- structure on the Atlantic Meridional Transect: a comparison between seasons. *Prog.*
- 926 Oceanogr., **45**, 369-386.
- 27 Zwirglmaier, K., Heywood, J. L., Chamberlain, K., Woodward, E. M. S., Zubkov, M. V. and
- Scanlan, D. J. (2007). Basin-scale distribution patterns of picocyanobacterial lineages in the
- 929 Atlantic Ocean. Environ. Microbiol., 9, 1278-1290.
- 200 Zwirglmaier, K., Jardillier, L., Ostrowski, M., Mazard, S., Garczarek, L., Vaulot, D., Not, F.,
- 931 Massana, R. et al. (2008) Global phylogeography of marine Synechococcus and
- *Prochlorococcus* reveals a distinct partitioning of lineages among oceanic biomes. *Environ*.
- 933 *Microbiol.*, **10**, 147-161.

Table I. Summary of data for each Lagrangian cycle. Surface NO_3^- and NH_4^+ are averaged across days within a cycle. NPP, NO_3^- and f-ratio are vertically integrated values. f-ratio = NO_3^- uptake / (NH_4^+ uptake + NO_3^- uptake) is a blended product that combines shipboard NO_3^- and ammonium uptake experiments (more accurate) with *in situ* NO_3^- uptake and NPP measurements (greater depth resolution).

	Cycle 1	Cycle 2	Cycle 3	Cycle 4	Cycle 5
Surface NO ₃ -					
(μΜ)	< 0.1	< 0.1	<0.1	< 0.1	< 0.1
Surface NH ₄ ⁺					
(μΜ)	< 0.025	< 0.025	< 0.025	< 0.025	0.025
Surface Chl a					
(µg/L)	0.107±0.04	0.049	0.080±0.007	0.100±0.01	0.127±0.01
NPP					
(mmol C m ⁻² d ⁻¹)	25.6±0.1	24.4±2.8	24.9±0.4	29.2±3.0	30.1± 2.9
In Situ NO ₃ -					
Uptake					
(μmol N m ⁻² d ⁻¹)	3.45±1.63	1.49±0.21	0.99±0.37	0.74 ± 0.02	1.48±0.09
<i>f</i> -ratio	0.22	0.02	0.05	0.06	0.12

Table II. Summary of *in situ* observations. Group-specific biomass are vertically integrated to the base of the euphotic zone for each Lagrangian cycle. Units are mmol N m⁻² (converted from carbon-based values reported in Selph *et al.* (this issue) by dividing by a Redfield C:N ratio of 106:16, mol:mol). Values marked with NM were not measured.

	Cycle 1	Cycle 2	Cycle 3	Cycle 4	Cycle 5
Prochlorococcus	6.16 ± 0.22	6.76 ± 0.28	6.85 ± 0.37	4.85 ± 0.04	3.24 ± 0.45
Synechococcus	1.44 ± 0.04	1.25 ± 0.03	1.22 ± 0.04	2.57 ± 0.05	2.36 ± 0.37
Diatom	0.26 ± 0.11	NM	NM	0.07 ± 0.004	0.04 ± 0.003
Dinoflagellate	0.47 ± 0.05	NM	NM	0.40 ± 0.11	0.43 ± 0.02
Prymnesiophytes	0.33 ± 0.03	NM	NM	0.44 ± 0.18	0.54 ± 0.03
Other Eukaryotes	2.46 ± 0.84	0.79 ± 0.0	0.60 ± 0.0	0.47 ± 0.11	1.64± 0.5

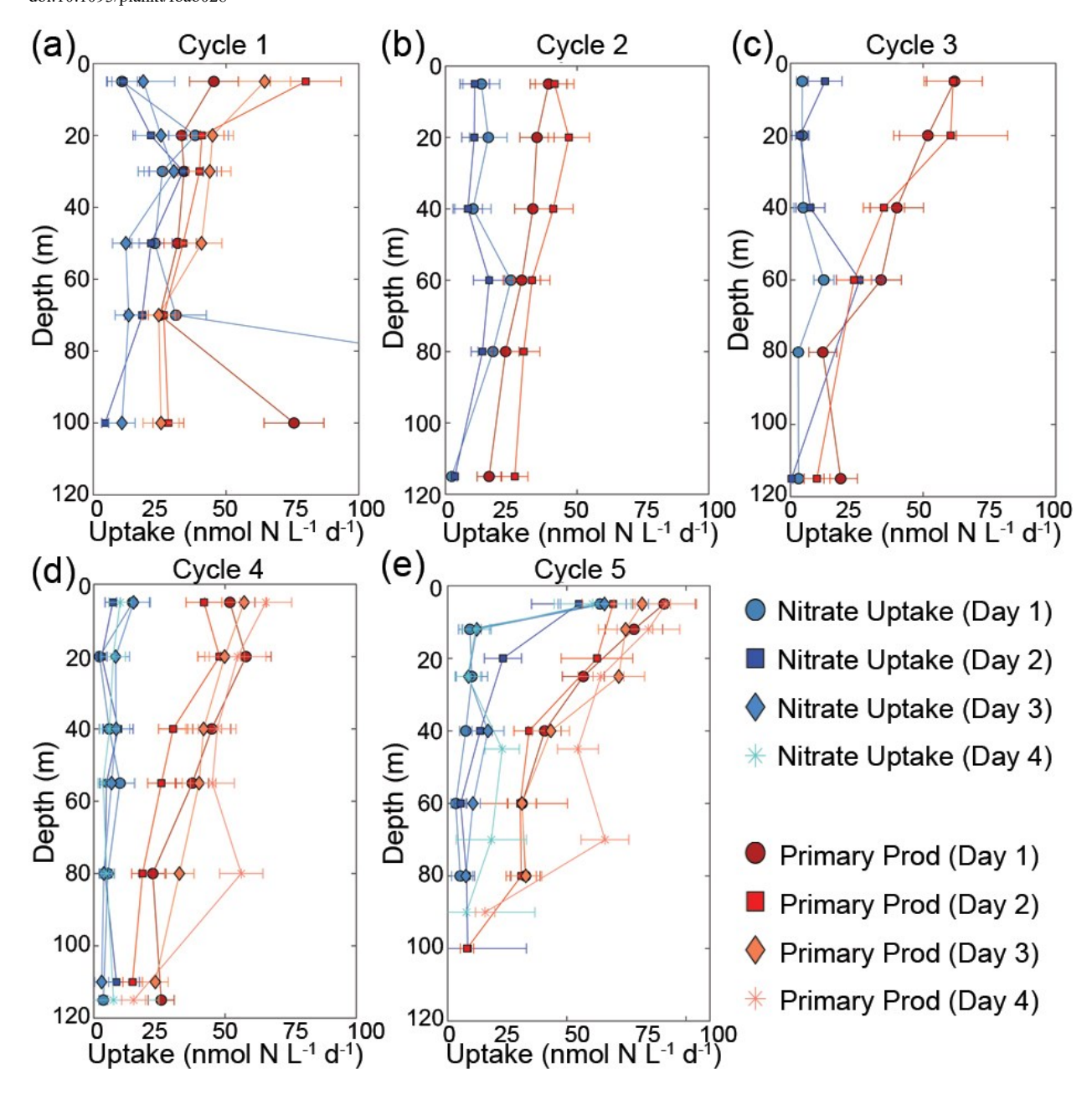


Figure 1. NO₃⁻ (red) and HCO₃⁻ uptake (blue) rates from *in situ* incubations. HCO₃⁻ uptake rates are converted to nitrogen units assuming Redfield ratio (6.625 molar ratios of C:N). Error bars represent 1 standard deviation of the mean.

972

973

974

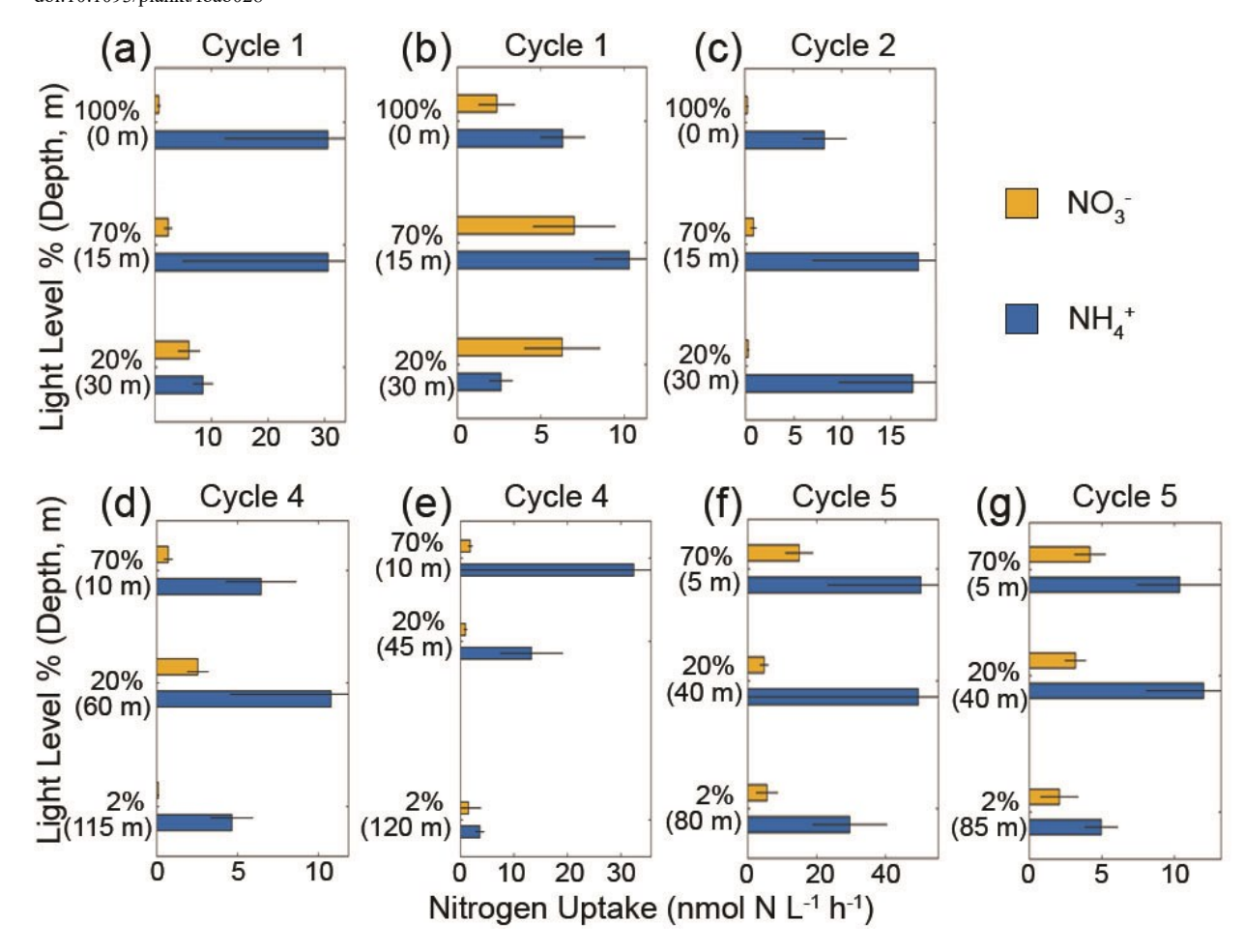


Figure 2. Results from NO₃⁻ (blue) and NH₄⁺ (orange) uptake experiments conducted shipboard at three light levels and water collection depth (m) as indicated. Error bars are replicate measurements.

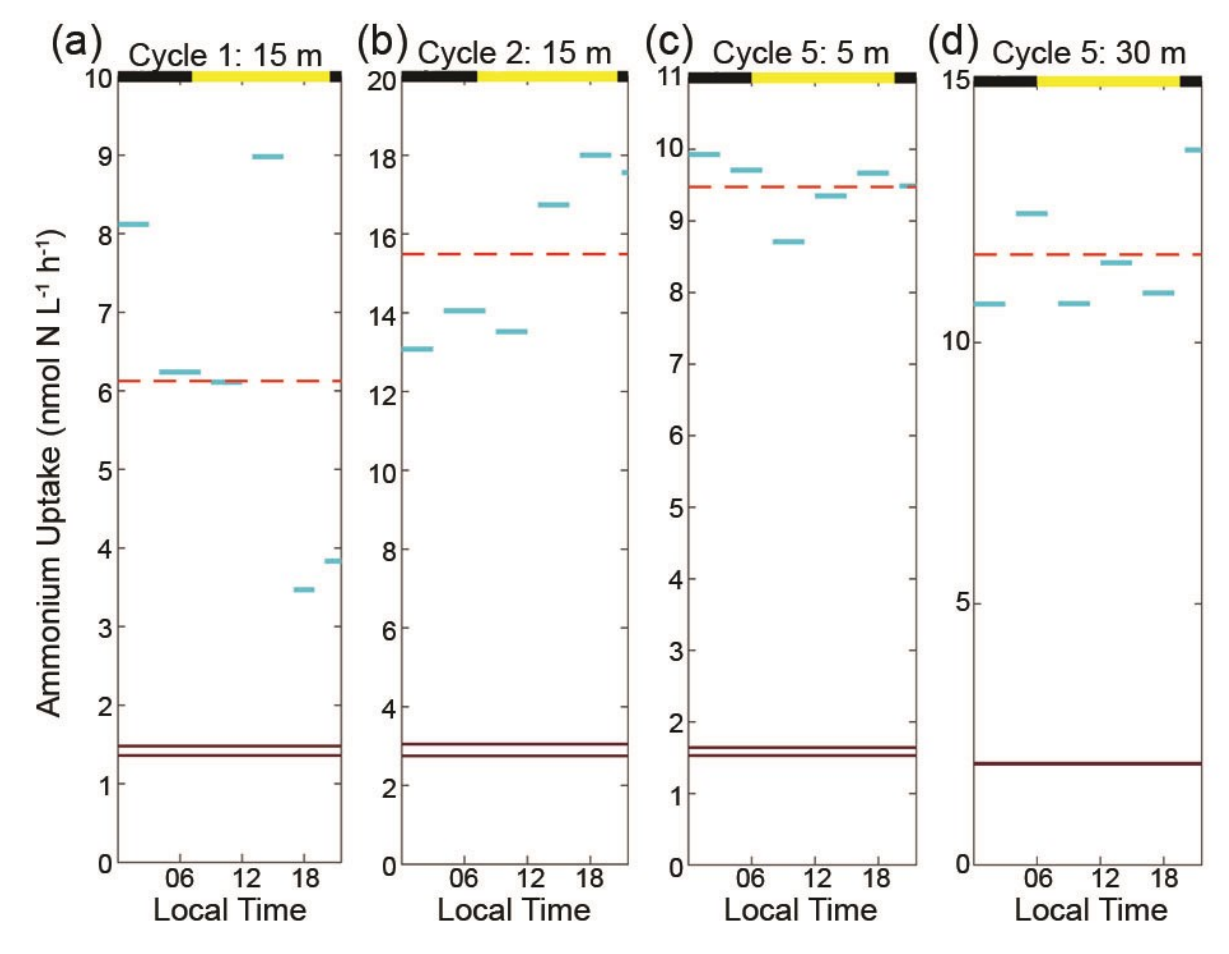


Figure 3. Diel NH₄⁺ uptake rates (nmol N L⁻¹ h⁻¹) with solid horizontal lines showing the duration and mean uptake rates for the 4-5 h (blue) and 24-h (dark brown) incubations. Dashed horizontal lines (orange) represent averages of 4-5-h incubations for comparison with 24-h incubations carried out during the same time frame. Black and yellow alternating bars (top of each figure) represent local daylight and dark hours. Depths indicate depth of water collection and approximate correspondence to incubator light level.

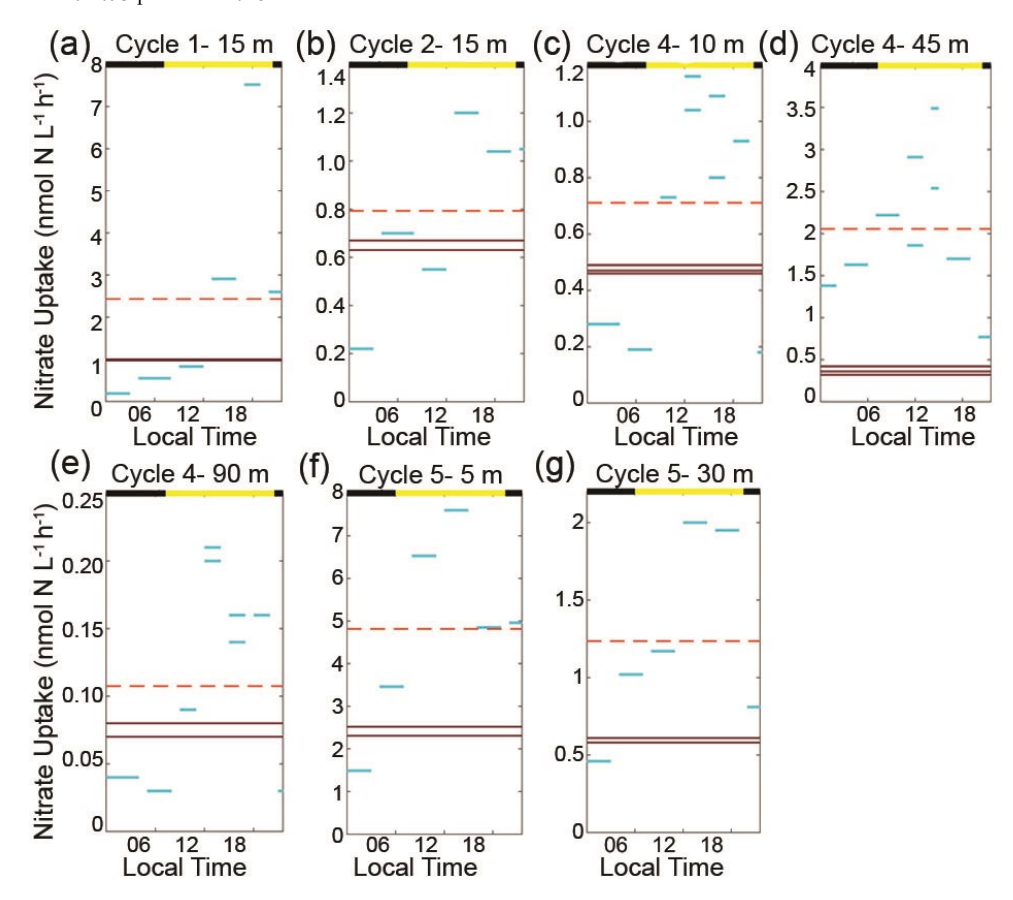


Figure 4. Diel NO₃⁻ uptake rates (nmol N L⁻¹ h⁻¹). Depths of water collection for the incubations are indicated next to the cycle number. Solid horizontal lines show the duration and mean uptake rates for the 4-5-h (blue) and 24-h (dark brown) incubations. Dashed horizontal lines (orange) represent averages of 4-5-h incubations for comparison with 24-h incubations carried out during the same time frame. Time periods that had more than one replicate are both shown, e.g, two blue lines at one time period. Black and yellow alternating bars (top of each figure) represent local daylight and dark hours.

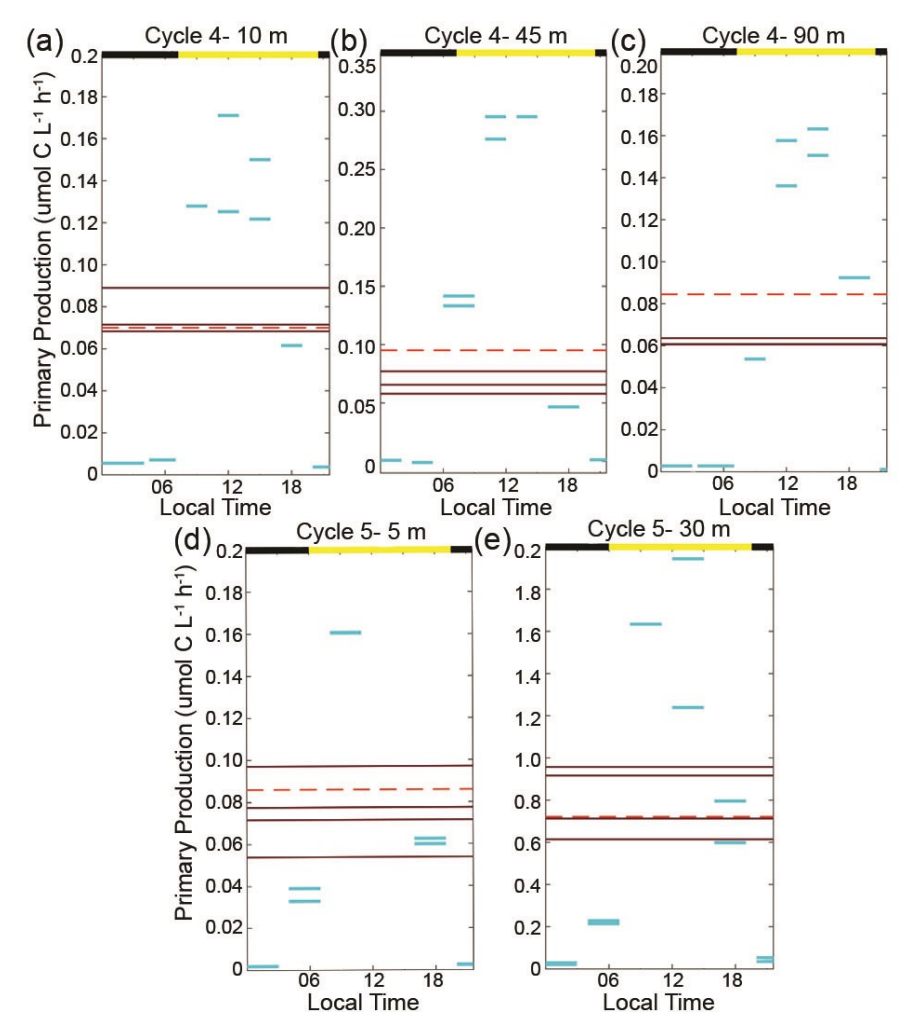


Figure 5. Diel primary production (μmol C L⁻¹ h⁻¹) from shipboard experiments. Solid horizontal lines show the duration and uptake rates for individual 4-5 h (blue) and duplicate 24-h (dark brown) incubations. Time periods that had more than one replicate are both shown, e.g, two blue lines at one time period. Dashed horizontal lines (orange) represent averaged short incubations for comparison with 24-hour incubations. Black and yellow bars located at the top of figures represents local daytime and nighttime.

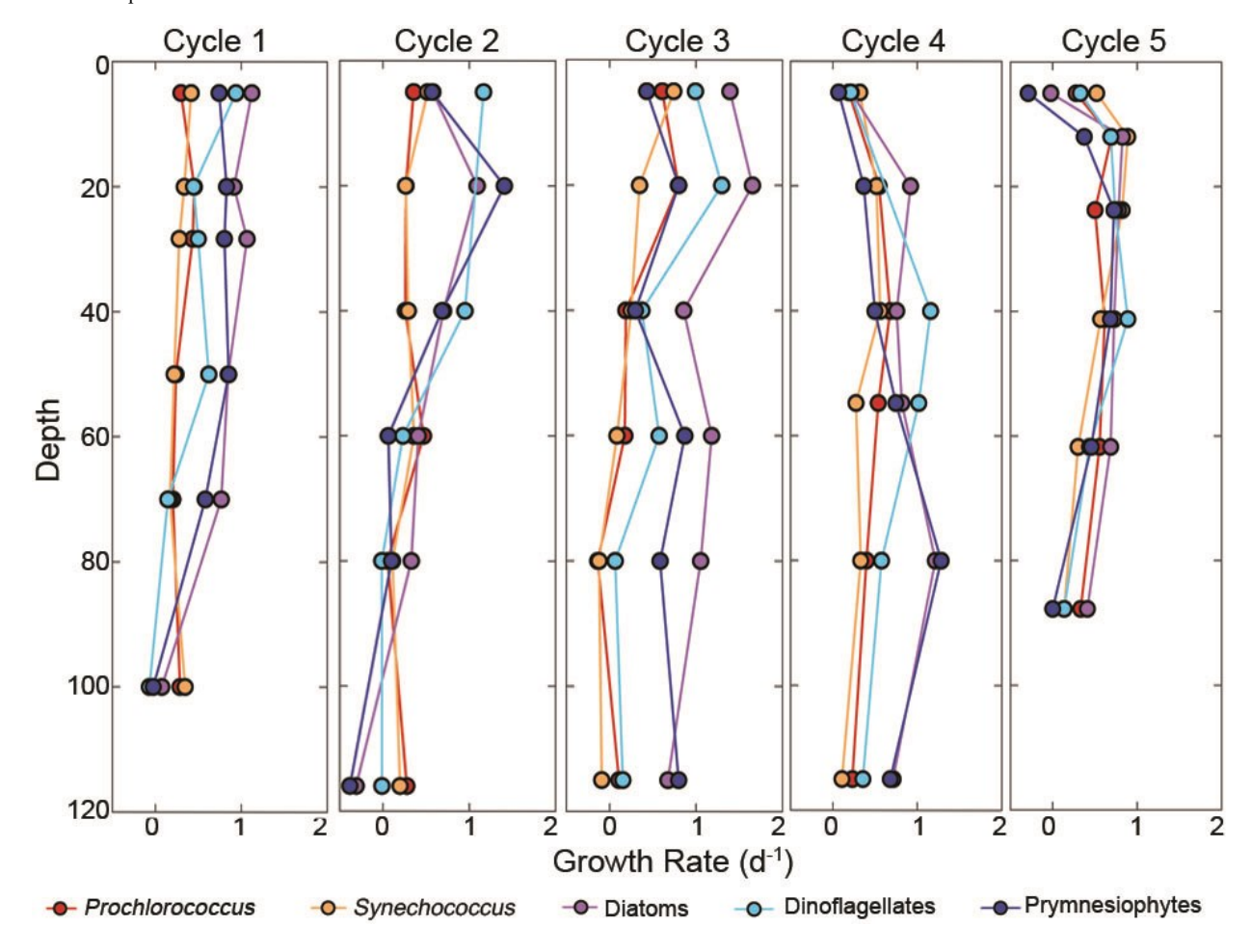


Figure 6. Dilution experiment results from cycles 1-5, showing averaged group-specific growth rates for *Prochlorococcus*, *Synechococcus*, diatoms, dinoflagellates and prymnesiophytes as a function of depth. Details of experiments are in Landry *et al.*, this issue.

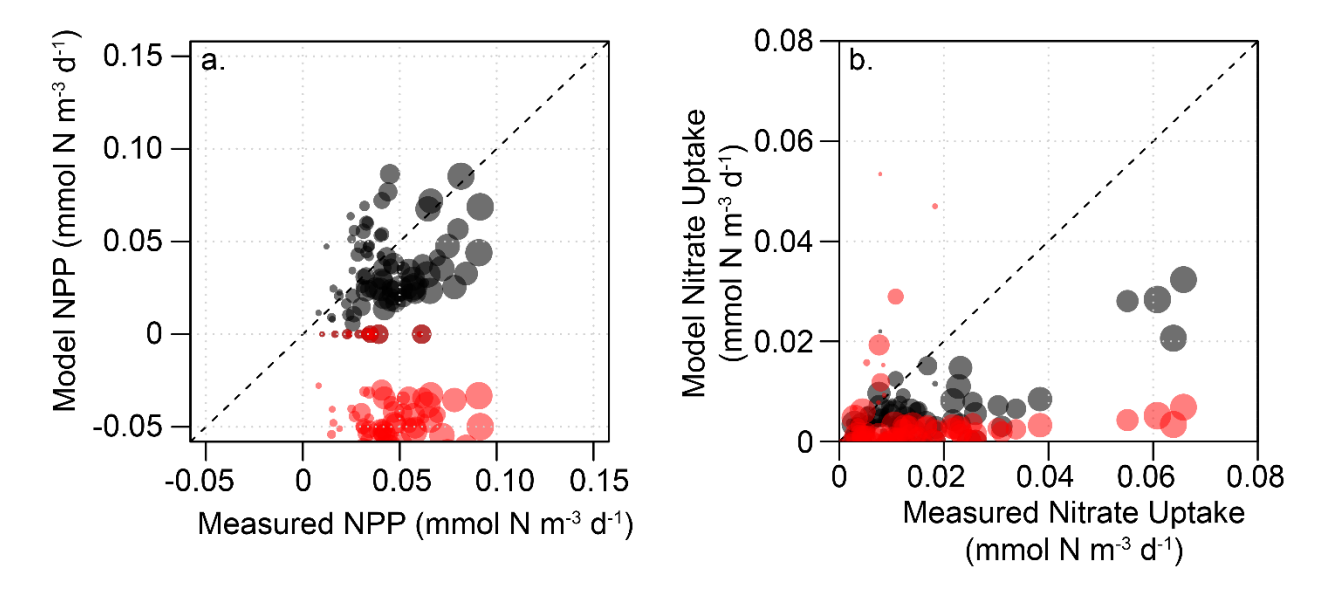


Figure 7. Model-observation comparisons for (a) NPP and (b) NO₃⁻ uptake. The dashed line represents the 1:1 ratio. Red dots indicate NEMURO-GoM parameterization while black dots show the "optimized" parameterization.

1012

1013

10141015

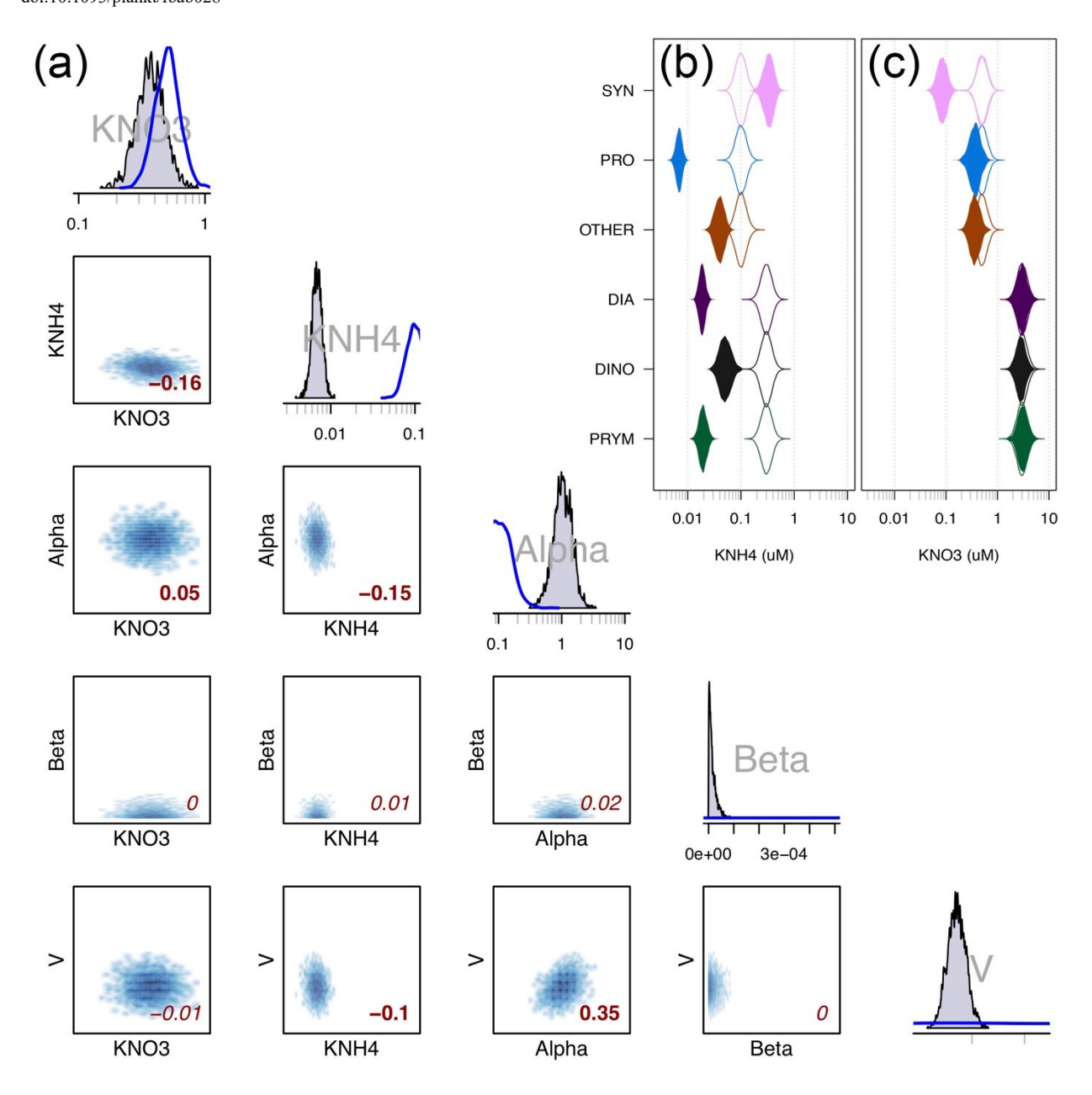


Figure 8. (a) Model parameters of log-transformed K_{NH4} (μmol L^{-1}), log-transformed K_{NO3} (μmol L^{-1}), log-transformed Alpha (m^2 W^{-1} d^{-1}), Beta (m^2 W^{-1} d^{-1}) and log-transformed V at 0°C (d^{-1}) for *Prochlorococcus*. Upper plots are histograms for each variable (filled gray lines, $n = 10^6$, subsampled to 2×10^4), with blue lines approximating the prior distribution that was assumed for each variable from previous studies. Lower property-property plots show the correlation between any two parameters (note that scales are as in the histograms above). Red value located in bottom right corner in each subplot gives Pearson's correlation coefficient (which is suitable for use with non-normal data, Nefzger and Drazow, 1957), with bold values indicating significance at p < 0.05. Violin plots of (**b**) NH₄⁺ half-saturation constants (K_{NH4} , μM) and (**c**) NO₃⁻ half-saturation constants (K_{NO3} , μM) from the optimized model (filled) and their priors

1028 (empty).

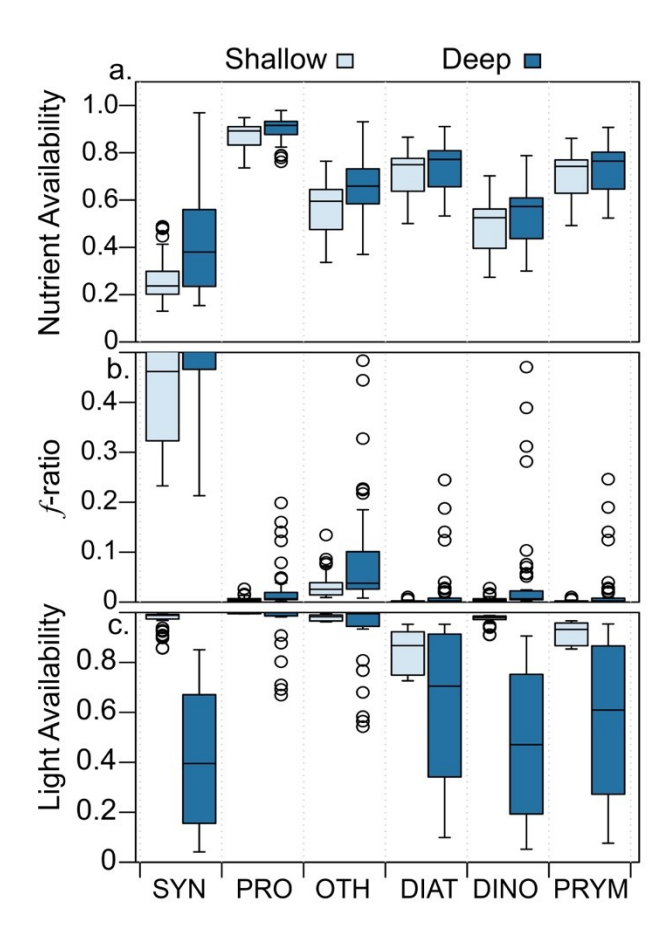


Figure 9. Modeled results for each phytoplankton group for (a) nutrient availability (unitless growth rate multiplier equal to NL + AL in Eqs. 1 and 2), (b) *f*-ratio and (c) light availability (unitless growth rate multiplier equal to LL in Eq.) as a function of depth. Light bars represent shallow water (< 50 m) and dark bars represent deeper samples (>50 m). Note that the upper quartile and 95% C.I. values are offscale for SYN in panel b with values of 0.551 and 0.696 for shallow and 0.699 and 0.921 for deep. See equations 1-4 for formulas and additional information on the calculations.